

NACA RM-450-117



~~SECRET~~
C.2

RESEARCH MEMORANDUM

WIND-TUNNEL INVESTIGATION OF THE LOW-SPEED LONGITUDINAL
AND LATERAL CONTROL CHARACTERISTICS OF A TRIANGULAR-
WING MODEL OF ASPECT RATIO 2.31 HAVING
CONSTANT-CHORD CONTROL SURFACES

By Walter D. Wolhart and William H. Michael, Jr.

Langley Aeronautical Laboratory
Langley Air Force Base, Va.

CLASSIFICATION CANCELLED

Authority: J. W. Crowley 12/11/53

EO 1.059.10

By: [Signature] 1/8/54 ses [Signature]

CLASSIFIED DOCUMENT # 9 18 235

This document contains classified information affecting the national defense of the United States within the meaning of the Espionage Act, USC 5031 and 32. Its transmission or the revelation of its contents in any manner to an unauthorized person is prohibited by law. Information so classified may be imparted only to persons in the military and naval services of the United States, appropriate civilian officers and employees of the Federal Government who have a legitimate interest therein, and to United States citizens of known loyalty and discretion who of necessity must be informed thereof.

NATIONAL ADVISORY COMMITTEE FOR AERONAUTICS

WASHINGTON
September 6, 1950

UNCLASSIFIED

NATIONAL ADVISORY COMMITTEE FOR AERONAUTICS

RESEARCH MEMORANDUM

WIND-TUNNEL INVESTIGATION OF THE LOW-SPEED LONGITUDINAL
AND LATERAL CONTROL CHARACTERISTICS OF A TRIANGULAR-
WING MODEL OF ASPECT RATIO 2.31 HAVING
CONSTANT-CHORD CONTROL SURFACES

By Walter D. Wolhart and William H. Michael, Jr.

SUMMARY

A wind-tunnel investigation has been made to determine the low-speed longitudinal and lateral control characteristics of a model with a triangular wing having NACA 65(06)-006.5 airfoil sections and aspect ratio 2.31 and equipped with constant-chord control surfaces.

The results indicate that the hinge moments of such a model are of somewhat larger magnitude than would be expected for unswept wings of comparable aspect ratio. Modifications to the plan form of the control surface near the wing tips had a rather critical effect on the hinge-moment parameters but had a smaller effect on the control effectiveness. Addition of the fuselage to the wing tended to increase both the effectiveness and the hinge moments of the control surfaces. The hinge-moment parameters were approximately the same whether the control surfaces were deflected symmetrically or asymmetrically.

Small effects were obtained by sealing the gap at the nose of the control surface, adding transition strips at the wing leading edge, or varying the Reynolds number over a limited range.

INTRODUCTION

Low-aspect-ratio wings of triangular plan form have been proposed in reference 1 and elsewhere as aerodynamically and structurally suitable for high-speed flight. One means of control for such wings has been supplied by some type of trailing-edge control surface. Theoretical analyses of the characteristics of such control surfaces at supersonic speeds are given in references 2 and 3. No suitable theory is available

for subsonic speeds, although some experimental results on the hinge-moments and effectiveness of constant-chord trailing-edge controls on a triangular wing of aspect ratio 2 are given in reference 4 for 5-percent-thick, double-wedge airfoil sections and in reference 5 for modified NACA 0005 airfoil sections. Some additional data on the effectiveness of such controls on triangular wings are given in reference 6 for a wing of aspect ratio 2.31 having 10-percent-thick biconvex airfoil sections, and in reference 7 for a wing of aspect ratio 2 having 5-percent-thick double-wedge airfoil sections and equipped with split flaps.

The present investigation was conducted in order to extend the available information on the factors contributing to the low-speed control characteristics of triangular wings. The investigation included determination of the effects on the longitudinal and lateral control characteristics of adding a fuselage and vertical tail to a wing, modifying the plan form of the control surfaces near the wing tips, adding transition strips, varying the Reynolds number over a limited range, and sealing the gap at the nose of the control surface.

SYMBOLS

The data presented herein are in the form of standard NACA coefficients of forces and moments which are referred to the stability system of axes with the origin at the quarter-chord point of the mean aerodynamic chord. The positive direction of forces, moments, and angular displacements are shown in figure 1. The coefficients and symbols are defined as follows:

C_L	lift coefficient (L/qS)
C_X	longitudinal-force coefficient (X/qS); $C_X = -C_D$ at $\psi = 0^\circ$
C_Y	lateral-force coefficient (Y/qS)
C_l	rolling-moment coefficient (L'/qSb)
C_m	pitching-moment coefficient ($M/qS\bar{c}$)
C_n	yawing-moment coefficient (N/qSb)
C_h	hinge-moment coefficient ($H/qb\bar{c}e^2$)
L	lift, pounds
X	longitudinal force, pounds

Y	lateral force due to deflection of right control surface (elevon) relative to the trim deflection $\delta_{e\text{trim}}$, pounds
L'	rolling moment due to deflection of right control surface (elevon) relative to trim deflection $\delta_{e\text{trim}}$, foot-pounds
M	pitching moment, foot-pounds
N	yawing moment due to deflection of right control surface (elevon) relative to trim deflection $\delta_{e\text{trim}}$, foot-pounds
H	hinge moment, foot-pounds
A	aspect ratio (b^2/S)
b	span, feet
S	wing area, square feet
c	chord parallel to plane of symmetry, feet
\bar{c}	mean aerodynamic chord, feet $\left(\frac{2}{S} \int_0^{b/2} c^2 dy \right)$
b_e	elevon span measured along trailing edge, feet
\bar{c}_e	root-mean-square chord of elevon aft of hinge line, feet
R	Reynolds number $\left(\frac{\rho V \bar{c}}{\mu} \right)$
q	dynamic pressure $(\rho V^2/2)$
ρ	mass density of air, slugs per cubic foot
V	free-stream velocity, feet per second
μ	coefficient of viscosity of air, slugs per foot-second
α	angle of attack measured in plane of symmetry, degrees
δ_e	deflection of control surface (elevon) from wing-chord line, degrees
δ_{eR}	deflection of right control surface (elevon) from wing-chord line, degrees

δ_{trim} symmetrical deflection of both control surfaces (elevons),
degrees

Λ_{LE} angle of sweepback of wing leading edge, degrees

$\Lambda_{\text{c}/4}$ angle of sweepback of wing quarter-chord line, degrees

$$C_{L\alpha} = \frac{\partial C_L}{\partial \alpha}$$

$$C_{m\alpha} = \frac{\partial C_m}{\partial \alpha}$$

$$C_{h\alpha} = \frac{\partial C_h}{\partial \alpha}$$

$$C_{L\delta} = \frac{\partial C_L}{\partial \delta}$$

$$C_{m\delta} = \frac{\partial C_m}{\partial \delta}$$

$$C_{h\delta} = \frac{\partial C_h}{\partial \delta}$$

$$C_{l\delta} = \frac{\partial C_l}{\partial \delta}$$

$$\alpha_{\delta} = \frac{C_{L\delta}}{C_{L\alpha}}$$

APPARATUS, MODEL, AND TESTS

The tests were made in the 6- by 6-foot test section of the Langley stability tunnel. The model was mounted on a conventional six-component balance system with the pivot point located at the quarter-chord point of the mean aerodynamic chord.

All of the component parts of the model were constructed of laminated mahogany and were given highly polished surfaces. The principal dimensions of the model are given in figure 2 and table I. The wing tested was the same wing used in the investigation reported in reference 8 with modifications to provide for constant-chord partial-span control surfaces. The wing had a 60°-sweptback leading edge, an aspect

ratio of 2.31, and a basic 65(06)-006.5 airfoil section parallel to the plane of symmetry, modified to provide straight sides from the trailing edge to the point of tangency with the 70-percent-chord point. The resulting trailing-edge angle was 8° . The fuselage was of circular cross section and had a fineness ratio of 7.02. The vertical tail had a 60° -sweptback leading edge, a flat-plate profile with rounded leading edge and beveled trailing edge, and an aspect ratio of 1.15. The constant-chord trailing-edge control surfaces (elevons) were used for both longitudinal and lateral control. The elevons were constructed so that they could be deflected simultaneously or independently over an elevon-deflection range of $\pm 25^\circ$. Either the horn balance or the tip could be removed from the elevons and attached to the wing without changing the wing plan form. Hinge moments were measured by two strain-gage units installed in the right elevon. The elevons had a radius nose. For most of the tests a small gap (equal to 0.031 inch) was left open at the nose of the elevon; however, the effect of closing this gap by means of a grease seal was determined for one of the model configurations.

A photograph of the complete model with the horn-on elevon configuration is presented as figure 3.

The longitudinal-control effectiveness and hinge-moment characteristics were obtained from measurements of lift, pitching moment, and hinge moment over an angle-of-attack range from about -4° to 37° for a range of elevon deflections from -20° to 20° . The lateral-control effectiveness and hinge-moment characteristics were obtained from measurements of lateral force, yawing moment, rolling moment, and hinge moment throughout the angle-of-attack range with the left elevon set at a fixed deflection δ_{trim} and the right elevon deflection δ_{ep} varied. For most of the lateral-control tests the deflection δ_{trim} was 0° ; however, tests of the complete model with the horn-on elevon configuration were made with values of δ_{trim} of both 0° and -10° . The effect of adding transition strips at the wing leading edge was determined for the complete model with the horn-on elevon configuration. The transition strips were prepared by cementing No. 60 carborundum grains to Scotch cellulose tape 1/2 inch wide and applying at the wing leading edge. The effects of variation in Reynolds number from 1.62×10^6 to 2.62×10^6 were determined for the complete model with the horn-on elevon configuration. The Mach number and corresponding Reynolds numbers are given in table II.

CORRECTIONS

The angle of attack and longitudinal force have been corrected for the effect of jet boundaries. A blocking correction was applied to the dynamic pressure by using the method described in reference 9. No tare corrections have been applied to the data; however, from previous investigations, these corrections are believed to be small. The effect of elevon deflection due to aerodynamic loading is not included in the data, but static tests indicate this correction would be very small.

RESULTS AND DISCUSSION

Presentation of Results

In the present paper, data on the longitudinal and lateral control characteristics have been presented separately for convenience in discussing the results.

The data are presented as indicated in the following table:

	Figures
Longitudinal characteristics:	
Basic data	4 to 11
Effect of elevon plan-form modifications	12
Effect of Reynolds number and transition strips	13 to 14
Effect of elevon nose seal	15
Lateral characteristics:	
Basic data	16 to 20
Effect of elevon plan-form modifications	21
Effect of elevon-trim deflection	22

Some of the important effectiveness and hinge-moment parameters are presented in table II to enable a more direct comparison of results.

Longitudinal Characteristics

Basic data.- The results obtained for the wing alone (fig. 4) show that the effectiveness of the elevons in producing lift and pitching moment generally decreased at large positive elevon deflections and at the high angles of attack. The irregularities which appear in the lift and pitching-moment curves become more severe for positive elevon deflection. Irregularities of this type have been noted in previous investigations such as those reported in references 4, 6, and 7.

The variation of hinge-moment coefficient with angle of attack is negative and approximately linear below the angle of attack corresponding to the initial break in the pitching-moment curve. The slopes of the hinge-moment curves generally become increasingly negative as the angle of attack is increased beyond this point. For low and moderate angles of attack, the divergence of the hinge-moment curves at elevon deflections greater than $\delta_e = \pm 10^\circ$ shows a nonlinear variation of hinge-moment coefficient with elevon deflection for large deflections.

The longitudinal-force curves are smooth throughout the angle-of-attack range, but the variation of C_x with angle of attack increases quite rapidly at low angles of attack when the elevons are deflected to increase the lift. The longitudinal-force curves are presented only for the wing-alone configuration, but tunnel plots indicated that while addition of the fuselage to the wing increased the minimum value of C_x it did not change the general character of the curves.

A comparison of wing-alone results with complete-model results (figs. 4 and 5) shows that adding the fuselage had little effect on the general character of the lift, pitching-moment, or hinge-moment curves, although the maximum lift coefficient decreased (with elevons neutral, the maximum lift coefficient decreased from 1.22 to 1.15). A similar effect of the fuselage on the maximum lift coefficient is noted in reference 8. Adding the fuselage increased the effectiveness parameters $C_{L\delta}$ and $C_{m\delta}$ and the hinge-moment parameters $C_{h\alpha}$ and $C_{h\delta}$ (table II).

Effect of elevon plan-form modifications. - The effect of elevon plan-form modifications on the complete model is shown in figure 12. Removing the horn balance increased $C_{h\alpha}$ from -0.0075 to -0.0084 and $C_{h\delta}$ from -0.0102 to -0.0108. Removing the elevon tip reduced $C_{h\alpha}$ and $C_{h\delta}$ to -0.0040 and -0.0085, respectively. It appears therefore that the elevon tip plan form has rather large effects on the hinge-moment parameters, although as shown in table II, the tips had relatively small effects on the longitudinal effectiveness parameters $C_{L\delta}$ and $C_{m\delta}$.

The hinge-moment parameters obtained for the complete model with the horn-off elevon configuration might be compared with similar parameters obtained from tests of constant-chord trailing-edge control surfaces on triangular wings of aspect ratio 2, such as those reported in reference 4 for 5-percent-thick double-wedge airfoil sections and in reference 5 for modified NACA 0005 airfoil section (modified to the extent that aft of the 67-percent-chord point the sections were faired to the trailing edge by straight lines). The wings of aspect ratio 2 were tested without a fuselage and were equipped with full-span constant-chord control surfaces having a radius nose, no aerodynamic balance, and

a ratio of control area to wing area of 0.20. The wing of reference 4 had a trailing-edge angle of 3.6° and an open nose gap (equal to 0.37 percent of elevon chord); whereas the wing of reference 5 had a trailing-edge angle of 5.7° and sealed nose gap. The tests of both references 4 and 5 were run at a Reynolds number of approximately 15×10^6 . The comparison is shown in the following table, in which the values given for the model of the present investigation are for the complete model with the horn-off elevon configuration:

Parameter	Present triangular-wing model, A = 2.31	Triangular wings, A = 2	
		Reference 4	Reference 5
C_{h_α}	-0.0084	-0.0082	-0.0068
C_{h_δ}	-.0108	-.0135	-.0107

In general the values of C_{h_α} and C_{h_δ} for the triangular-wing model of aspect ratio 2.31 are in good agreement with values obtained for the triangular wings of aspect ratio 2. It is believed that the value of C_{h_α} from reference 5 would have been in better agreement had the elevon nose gap been unsealed. The somewhat larger value of C_{h_δ} from reference 4 is at least partly attributed to the usual effect of trailing-edge angle on C_{h_δ} (reference 10). Although, as noted, differences do exist in the test models and test conditions, it is believed that the results considered are a good indication of the hinge-moment-parameter values that might be expected at low speed on similar triangular wings having similar trailing-edge control surfaces.

The hinge-moment parameter obtained for the present triangular-wing model might also be compared with similar parameters obtained from tests of flaps on low-aspect-ratio unswept wings such as those reported in references 11 and 12. The unswept wings had an NACA 64A010 airfoil section, trailing-edge angle of 11° , and a ratio of flap area to wing area of 0.279. The present triangular-wing model had a trailing-edge angle of 8° , and the area of the elevon (if assumed to extend over the entire trailing edge of the wing for the complete-model configuration) was equal to 21 percent of the wing area. The comparison is shown in the following table, in which the values given for the triangular-wing model are for the horn-off elevon configuration:

Parameter	Triangular-wing model, A = 2.31	Unswept-wing model	
		A = 2	A = 3
$C_{h\alpha}$	-0.0084	-0.0002	-0.0010
$C_{h\delta}$	-.0108	-.0073	-.0088

Both $C_{h\alpha}$ and $C_{h\delta}$ are more negative for the triangular-wing model; however, the most significant difference is in the hinge-moment parameter $C_{h\alpha}$. It should be noted that the models are comparable only with respect to aspect ratio since differences exist in trailing-edge angle, ratio of flap area to wing area, and flap-chord distribution. The high negative values of $C_{h\alpha}$ for the triangular-wing model are considered to result from the fact that the flap chord is equal to or nearly equal to the wing chord in the vicinity of the wing tips. The usual effects of a high ratio of flap chord to wing chord in increasing the values of the hinge-moment parameters is made more important in the case of a triangular-wing model because of the character of the span-load distribution. The results of pressure-distribution investigations (references 5 and 13) on triangular-wing models of aspect ratio 2 show that at small angles of attack the lift-curve slope of sections near the wing tips may be considerably higher than the average lift-curve slope for the wing. The load carried by elevons having chords equal to or nearly equal to the wing chord near the tip therefore would be expected to be high.

The pressure-distribution results of references 5 and 13 also show a rearward shift in the centers of pressure over the outboard sections of the wing at moderate angles of attack. This appears to be reflected in the slightly increased hinge-moment slopes shown for all elevon configurations of the present model at angles of attack greater than about 12° .

Effect of Reynolds number and transition strips.- The effects of Reynolds number and transition strips are shown in figures 13 and 14, respectively, for the complete model, with the horn-on elevon configuration. In general, varying the Reynolds number had rather small effects on the variation of lift and hinge-moment coefficient with either angle of attack or elevon deflection for the limited range of Reynolds numbers investigated. However, the effects which did appear were the most noticeable for the hinge-moment parameter $C_{h\alpha}$ and the effectiveness parameters $C_{L\delta}$ and $C_{m\delta}$, where an increase in Reynolds number resulted

in a decrease in the absolute magnitude of the parameters $C_{h\alpha}$, $C_{L\delta}$, and $C_{m\delta}$ as shown in table II.

Fixing transition strips to the wing leading edges resulted in a more linear variation of hinge-moment coefficient with angle of attack for the range between $\alpha = -4^\circ$ and $\alpha = 8^\circ$ and the elimination of the slight decrease in $C_{h\alpha}$ occurring at about $\alpha = 5^\circ$ with the transition strips off. However, when the decrease did occur at about $\alpha = 9^\circ$, it was of greater magnitude. Beyond $\alpha = 12^\circ$ the variation of hinge-moment coefficient with angle of attack was the same. Transition strips reduced the absolute value of the effectiveness parameters $C_{L\delta}$ and $C_{m\delta}$ but had no appreciable effect on the hinge-moment parameter $C_{h\delta}$ as shown in table II.

Effect of elevon nose seal.- The effect of sealing the small gap at the nose of the elevon is shown in figure 15 for the complete model with the tip-off elevon configuration. Sealing the elevon nose gap decreased the slope of the hinge-moment coefficient against angle-of-attack curve in the range between $\alpha = -4^\circ$ and $\alpha = 5^\circ$ and caused a small reduction in the magnitude of the hinge moments throughout the angle-of-attack range. There was a similar reduction in slope of the curve of hinge-moment coefficient against elevon deflection. Similar effects of nose-gap seal have been noted in previous investigations (fig. 14 of reference 10) when the trailing-edge angle is small. There was little effect of nose-gap seal on the effectiveness parameters $C_{L\delta}$ and $C_{m\delta}$ as shown in table II.

Lateral Characteristics

Basic data.- The results obtained for the wing alone are presented in figure 16 and show the variation of the lateral-force, yawing-moment, rolling-moment, and hinge-moment coefficients with angle of attack for various asymmetrical elevon deflections. For the lateral control characteristics, elevon deflection is regarded as the difference between the angles of the right and left elevons ($\delta_{eR} - \delta_{eTrim}$). These curves show that the elevon effectiveness in producing rolling moment generally became less with angle of attack. The initial breaks in the rolling-moment curves correspond to breaks in the pitching-moment curves and are probably caused by tip stalling. Deflecting the elevons to produce a rolling moment results in an adverse yawing moment due to a change in induced drag on the two wing panels. The adverse yawing moment increases with angle of attack and is generally largest for positive elevon deflections. The variation of lateral-force coefficient with elevon deflection is small and positive for all angles of attack below the stall. The

variation of hinge-moment coefficient with angle of attack is not changed appreciably by asymmetrical elevon deflections and the variation shows the same characteristics noted for symmetrical elevon deflections in the discussion on longitudinal characteristics.

A comparison of wing-alone results with complete-model results (figs. 16 and 17) shows that adding the fuselage to the wing resulted in a slight increase in rolling-moment effectiveness for angles of attack less than those corresponding to the breaks in the pitching-moment and hinge-moment curves, after which the rolling-moment effectiveness fell off more rapidly for the complete model. The increase in effectiveness at low angles of attack is at least partly attributed to the tendency for the fuselage to act as an end plate at the inboard end of the elevon and, therefore, to increase the loading due to elevon deflection in this region. Adding the fuselage and vertical tail to the wing caused a considerable increase in the lateral force due to elevon deflection and reduced the adverse yawing moment. The increased lateral force acting on the vertical tail produced favorable yawing moments up to about $\alpha = 4^\circ$ and generally reduced the adverse yawing moment for angles of attack below the stall.

Effect of elevon plan-form modifications.- The effect of elevon plan-form modifications on the complete model ($\delta_{\text{trim}} = 0^\circ$) is shown in figure 21. The variation of rolling-moment coefficient with elevon deflection is approximately linear for all three elevon configurations for the range of elevon deflections investigated. Removing either the horn balance or the tip generally reduced the rolling-moment effectiveness and changed the yawing moment due to elevon deflection. The curves of hinge-moment coefficient against elevon deflection show effects of elevon plan-form changes similar to those noted for symmetrical deflections; however, there were some changes in the hinge-moment parameter $C_{h\delta}$ (table II).

The rolling-moment coefficient against angle-of-attack curves are generally smoother for the tip off than either the horn-on or horn-off elevon configurations as shown by a comparison of figures 17, 18, and 19.

Effect of elevon-trim deflection.- The effect of elevon longitudinal trim deflection ($\delta_{\text{trim}} = -10^\circ$) at $\alpha = 0^\circ$ on the lateral control characteristics of the complete model with the horn-on elevon configuration is shown in figure 22. Changing the trim deflection to -10° decreased the rolling-moment effectiveness and was the most noticeable for negative elevon deflections ($\delta_{\text{ER}} - \delta_{\text{trim}}$) greater than -5° . The decrease in rolling-moment effectiveness is caused by partial stalling of the right elevon at the large negative deflections occurring with a trim deflection of -10° . The variation of lateral-force coefficient with elevon deflection decreases and the variation of yawing-moment

coefficient with elevon deflection increases, becoming more favorable for a trim deflection of -10° . The slope of the curve of hinge-moment coefficient against elevon deflection is less for a trim deflection of -10° than for a trim deflection of 0° in the elevon deflection ($\delta_{eR} - \delta_{e\text{trim}}$) range from -5° to 10° but shows a rapid increase at larger deflections.

For a trim deflection of -10° the rolling-moment effectiveness increases with angle of attack (at low and moderate angles of attack) for large negative elevon deflection as shown in figure 20. This is as expected since at the larger negative elevon deflection where the right elevon is partially stalled, any decrease in loading, such as would occur with an increase in angle of attack, increases the rolling-moment effectiveness.

A comparison of figures 17 and 20 also shows that favorable yawing moments are produced up to about $\alpha = 8^\circ$ for a trim deflection of -10° as compared with $\alpha = 4^\circ$ for a trim deflection of 0° .

Although the effect of elevon trim deflection on the lateral control characteristics of the complete model with the horn-on elevon configuration have been compared at $\alpha = 0^\circ$ in figure 22, it should be noted that for the present center-of-gravity location (25 percent of the mean aerodynamic chord) the model trims at an angle of attack of approximately 18° with $\delta_e = -10^\circ$ as shown in figure 5. With the model at an angle of attack of approximately 18° (with $\delta_e = -10^\circ$) the elevon rolling-moment effectiveness does not drop off as rapidly for negative elevon deflections ($\delta_{eR} - \delta_{e\text{trim}}$) greater than -5 as it did at $\alpha = 0^\circ$ (fig. 20) as mentioned previously. However, figure 20 also shows that the yawing moment is adverse for all elevon deflections investigated at $\alpha = 18^\circ$.

CONCLUSIONS

Results of a low-speed investigation of the longitudinal and lateral control characteristics of a triangular-wing model with constant-chord elevons indicate the following conclusions:

1. The values of the hinge-moment parameters were of somewhat greater magnitude than would be expected on unswept wings of comparable aspect ratio.

2. Modifications to the plan form of the control surface near the wing tips had a rather critical effect on the hinge-moment parameters but had a smaller effect on the control effectiveness.

3. Addition of the fuselage to the wing tended to increase both the effectiveness and the hinge moments of the elevons.

4. The elevon hinge-moment parameters were approximately the same whether the elevons were deflected symmetrically or asymmetrically.

5. The effects of sealing the elevon nose gap, adding transition strips at the wing leading edge, and varying the Reynolds number over a limited range were found to be rather small.

Langley Aeronautical Laboratory
National Advisory Committee for Aeronautics
Langley Air Force Base, Va.

REFERENCES

1. Jones, Robert T.: Properties of Low-Aspect-Ratio Pointed Wings at Speeds below and above the Speed of Sound. NACA Rep. 835, 1946.
2. Tucker, Warren A.: Characteristics of Thin Triangular Wings with Constant-Chord Full-Span Control Surfaces at Supersonic Speeds. NACA TN 1601, 1948.
3. Tucker, Warren A., and Nelson, Robert L.: Characteristics of Thin Triangular Wings with Constant-Chord Partial-Span Control Surfaces at Supersonic Speeds. NACA TN 1660, 1948.
4. Stephenson, Jack D., and Ameudo, Arthur R.: Tests of a Triangular Wing of Aspect Ratio 2 in the Ames 12-Foot Pressure Wind Tunnel. II - The Effectiveness and Hinge Moments of a Constant-Chord Plain Flap. NACA RM A8E03, 1948.
5. Graham, David: Chordwise and Spanwise Loadings Measured at Low Speeds on a Large Triangular Wing Having an Aspect Ratio of 2 and a Thin, Subsonic-Type Airfoil Section. NACA RM A50A04a, 1950.
6. Whittle, Edward F., Jr., and Lovell, J. Calvin: Full-Scale Investigation of an Equilateral Triangular Wing Having 10-Percent-Thick Biconvex Airfoil Sections. NACA RM L8G05, 1948.
7. Anderson, Adrien E.: An Investigation at Low Speed of a Large-Scale Triangular Wing of Aspect Ratio Two, - I. Characteristics of a Wing Having a Double-Wedge Airfoil Section with Maximum Thickness at 20-Percent Chord. NACA RM A7F06, 1947.
8. Jaquet, Byron M., and Brewer, Jack D.: Effects of Various Outboard and Central Fins on Low-Speed Static-Stability and Rolling Characteristics of a Triangular-Wing Model. NACA RM L9E18, 1949.
9. Herriot, John G.: Blockage Corrections for Three-Dimensional-Flow Closed-Throat Wind Tunnel, with Consideration of the Effect of Compressibility. NACA RM A7B28, 1947.
10. Langley Research Staff (Compiled by Thomas A. Toll): Summary of Lateral-Control Research. NACA Rep. 868, 1947.
11. Dods, Jules B., Jr.: Wind-Tunnel Investigation of Horizontal Tails. I - Unswept and 35° Swept-Back Plan Forms of Aspect Ratio 3. NACA RM A7K24, 1948.

12. Dods, Jules B., Jr.: Wind-Tunnel Investigation of Horizontal Tails. IV - Unswept Plan Form of Aspect Ratio 2 and a Two-Dimensional Model. NACA RM A8J21, 1948.
13. Anderson, Adrien E.: Chordwise and Spanwise Loadings Measured at Low Speed on Large Triangular Wings. NACA RM A9B17, 1949.

TABLE I.- MODEL GEOMETRIC DATA

Wing:	
Span, ft	3.04
Area, sq ft	4.0
Area exposed outside of fuselage, sq ft	2.47
Mean aerodynamic chord, ft	1.76
Aspect ratio	2.31
Sweepback (leading edge), deg	60
Sweepback (quarter-chord line), deg	52.2
Fuselage:	
Length, ft	4.68
Maximum diameter, ft67
Fineness ratio	7.02
Elevon:	
Area (total with horn on), sq ft333
Area (total aft of hinge line), sq ft326
Area (total with tip off), sq ft275
Root-mean-square chord (horn-on and horn-off elevon configurations), ft288
Root-mean-square chord (tip-off elevon configuration), ft296
Span (horn-on and horn-off elevon configuration), ft	1.188
Span (tip-off elevon configuration), ft927
Nose gap, percent of elevon chord87
Trailing-edge angle, deg	8.0
Vertical tail:	
Area, sq ft36
Aspect ratio	1.15

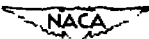

 NACA

TABLE II. - PARAMETER VALUES FOR 60° TRIANGULAR-WING MODEL WITH CONSTANT-CHORD ELEVONS

[Values measured at $\alpha = 0^\circ$, $\delta_e - \delta_{e\text{trim}} = 0^\circ$]

Model	Elevon	Reynolds number	Mach number	Elevon nose gap	Transition strips	$\delta_{e\text{trim}}$ (deg)	^a Longitudinal characteristics							^b Lateral characteristics			
							$C_{L\alpha}$	$C_{M\alpha}$	$C_{N\alpha}$	$C_{L\delta}$	$C_{M\delta}$	$C_{N\delta}$	$\alpha\delta$	$C_{Y\alpha}$	$C_{Y\delta}$	$C_{L\delta}$	
Wing Complete	Horn on	2.06×10^6	0.17	Open	off	0	0.040	-0.0048	-0.0072	0.017	-0.0082	-0.0099	0.425	-0.0072	-0.0094	-0.00183	
	↓	1.62×10^6	.13	↓	↓	↓	.042	-.0051	-.0084	.020	-.0096	-.0107	.476	-----	-----	-----	
		2.06×10^6	.17		On		.040	-.0047	-.0075	.019	-.0093	-.0102	.475	-.0073	-.0108	-.00197	
	↓	↓	↓	↓	↓	↓	-10	-----	-----	-----	-----	-----	-----	-----	-----	-----	-----
								off	.041	-.0050	-.0076	.018	-.0086	-.0103	.440	-----	-----
	↓	↓	↓	↓	↓	↓	0	.039	-.0049	-.0072	.018	-.0090	-.0103	.461	-----	-----	-----
								Horn off	2.06×10^6	.17	↓	.040	-.0048	-.0084	.018	-.0091	-.0108
↓	↓	↓	↓	↓	↓	↓	↓	↓	↓	↓	↓	↓	↓	↓	↓	↓	
																	Tip off
↓	↓	↓	↓	↓	↓	↓	.041	-.0052	-.0025	.018	-.0083	-.0080	.440	-----	-----	-----	

^aFor determining longitudinal control characteristics, both elevons are deflected symmetrically. Derivatives with respect to δ_e indicate changes in coefficients per degree deflection of either elevon.

^bFor determining lateral control characteristics, the left elevon is fixed at the deflection $\delta_{e\text{trim}}$. Derivatives with respect to δ_e indicate changes in coefficients per degree deflection of the right elevon.



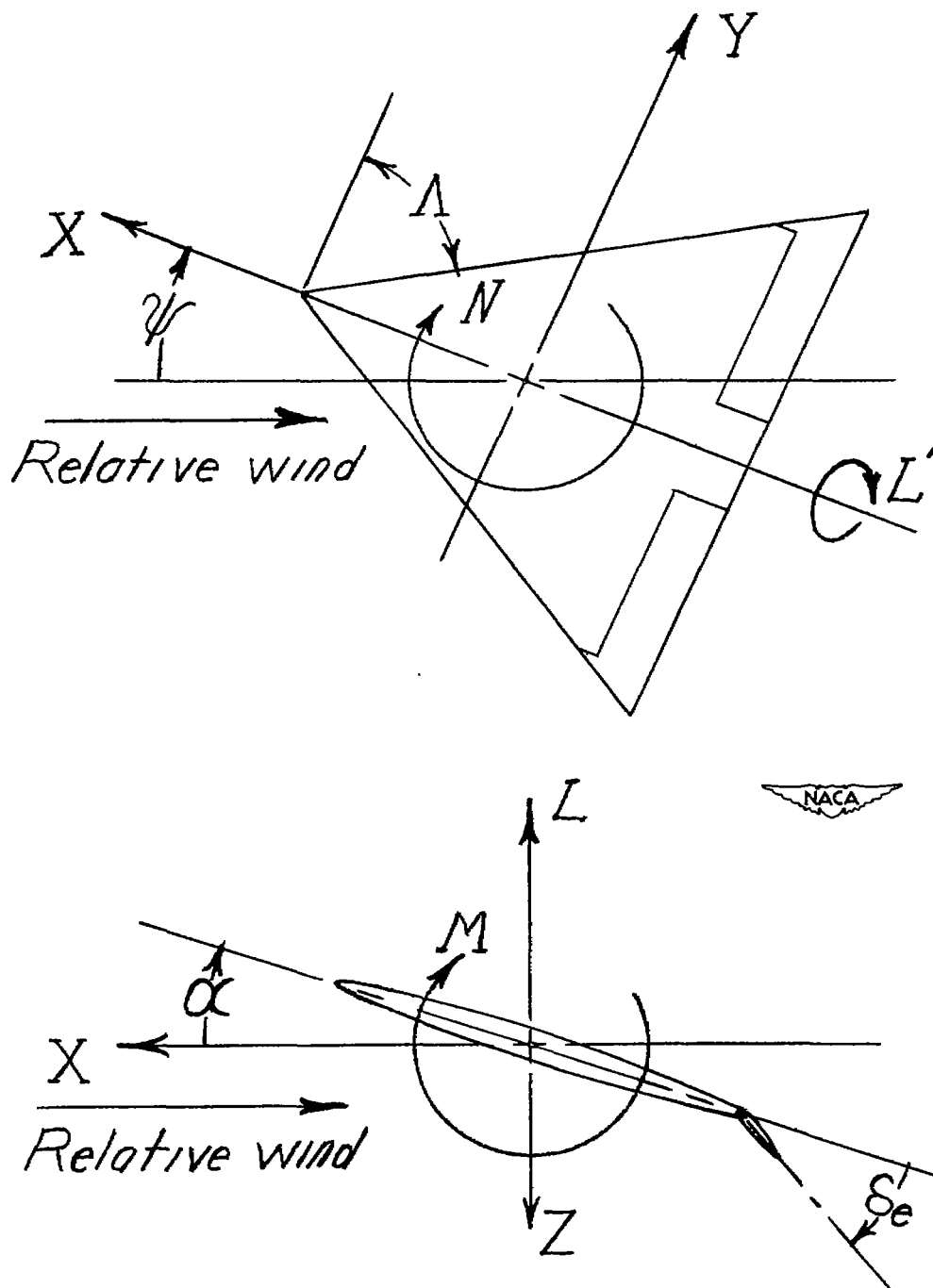


Figure 1.- System of stability axes. Positive forces, moments, and angles are indicated.

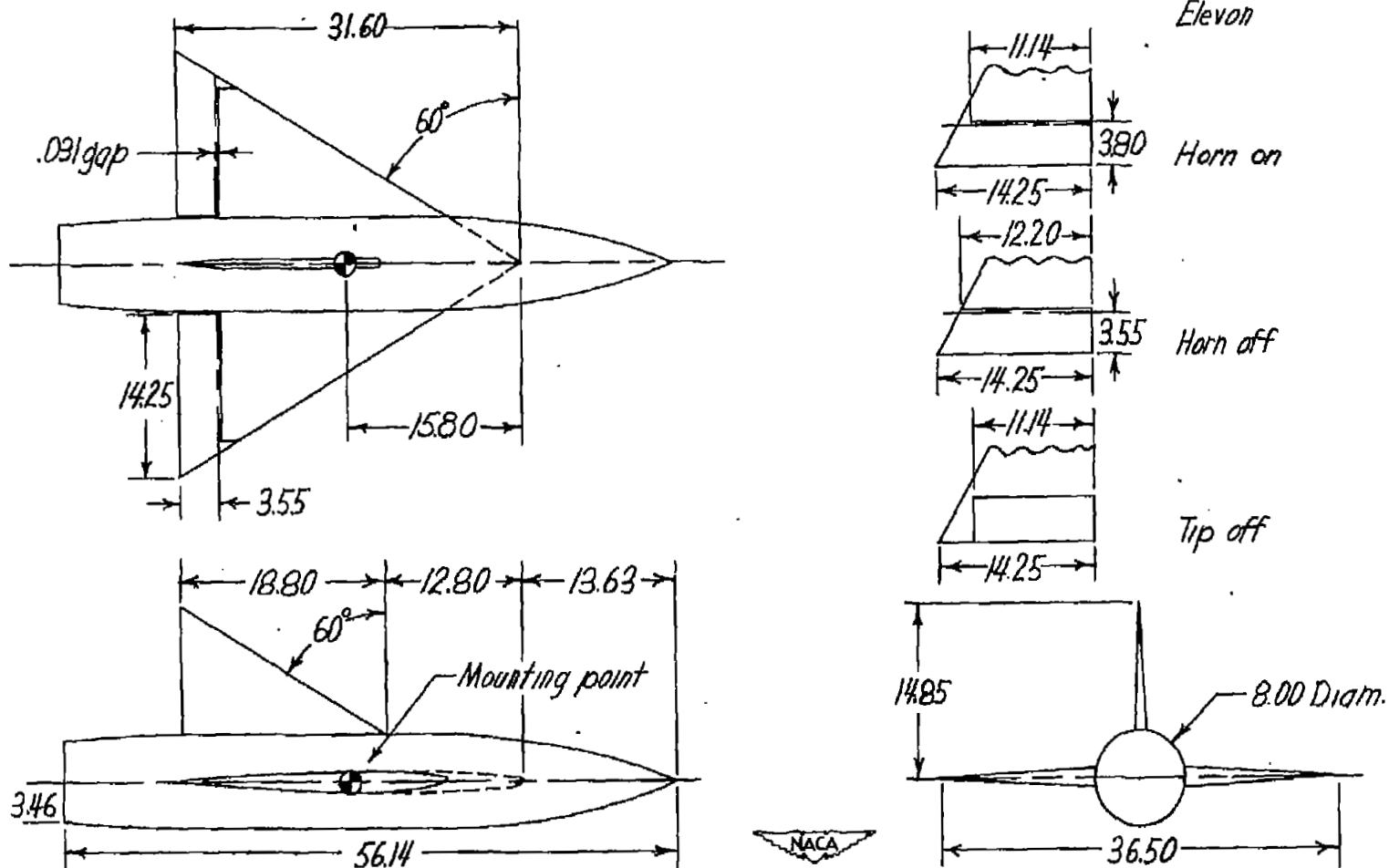


Figure 2.- Sketch of the complete model and elevon configurations investigated. (All dimensions in inches.)

11
12

13
14

15
16
17

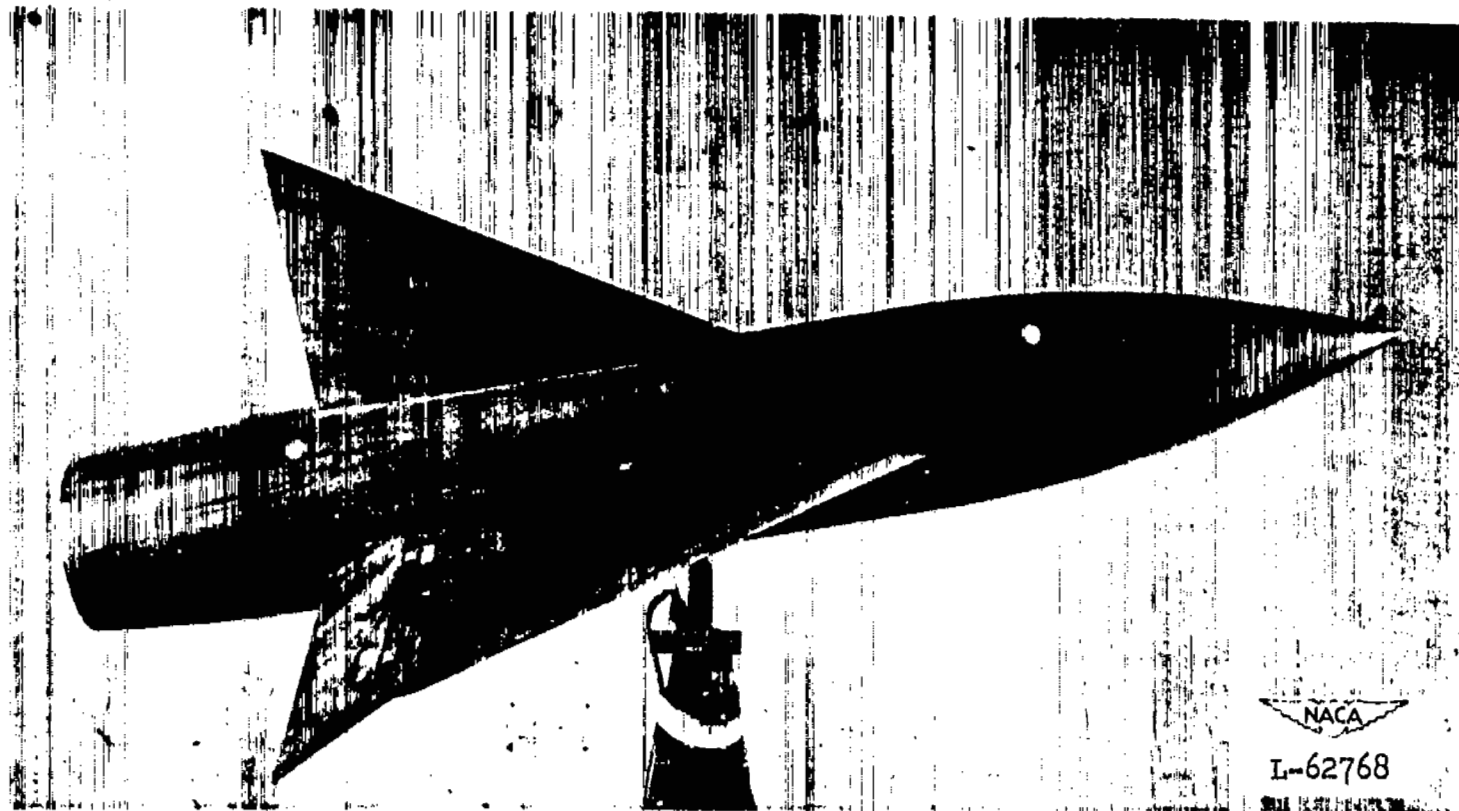
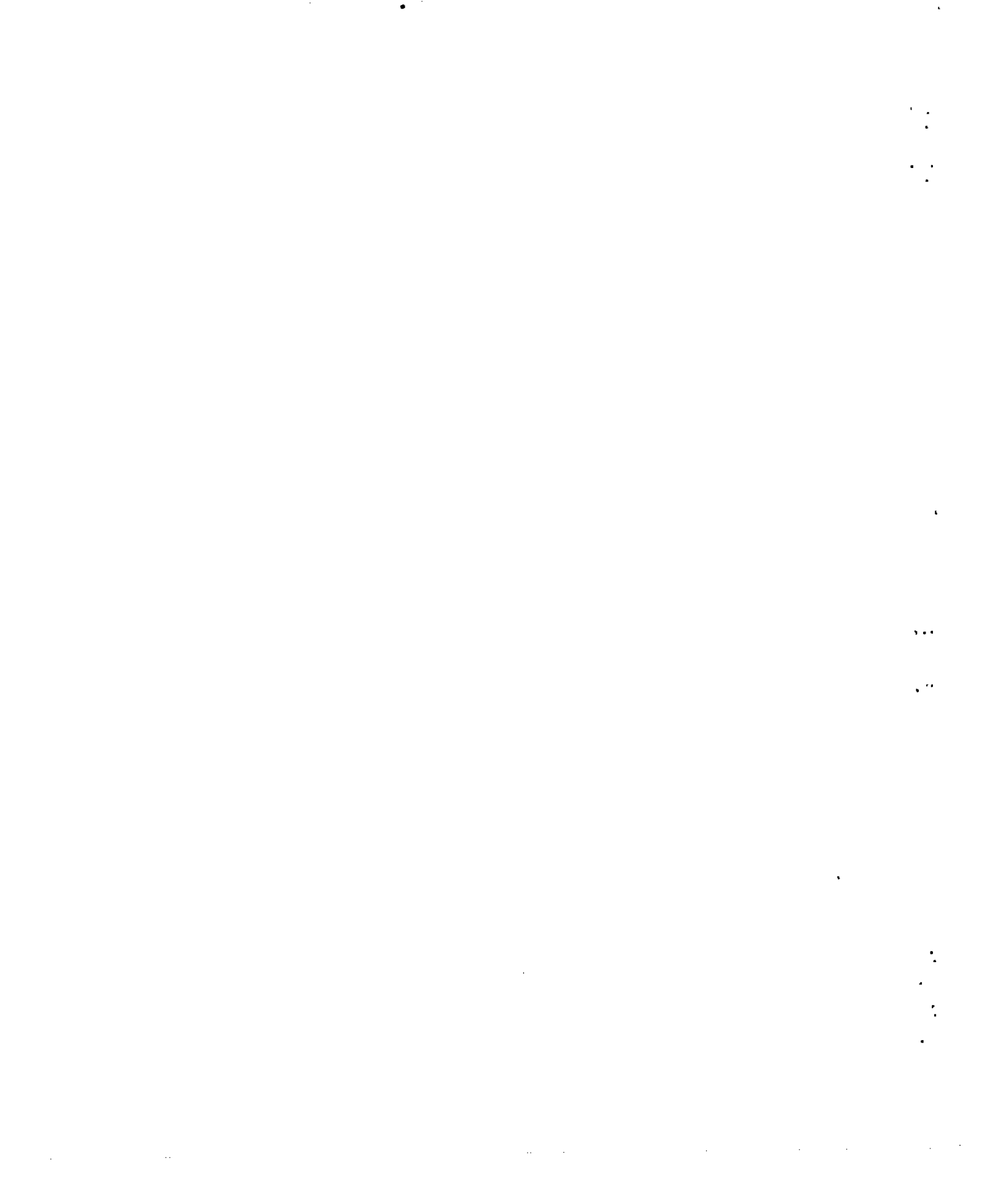


Figure 3.- Complete model with the horn-on elevon configuration mounted in Langley stability tunnel.



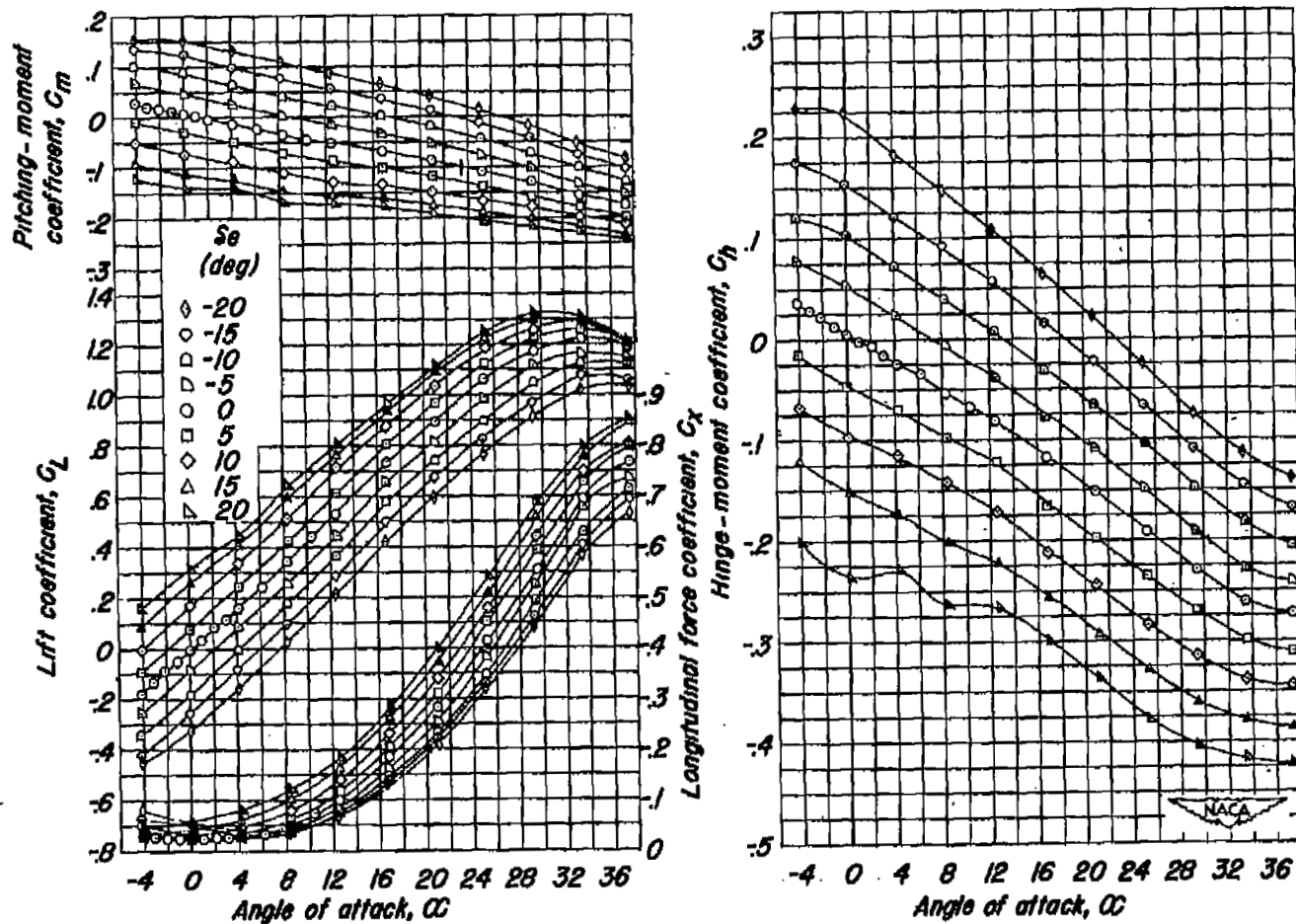


Figure 4.- Longitudinal control characteristics of wing alone. Elevon with horn on; $R = 2.06 \times 10^6$; transition strips off; elevon nose gap open.

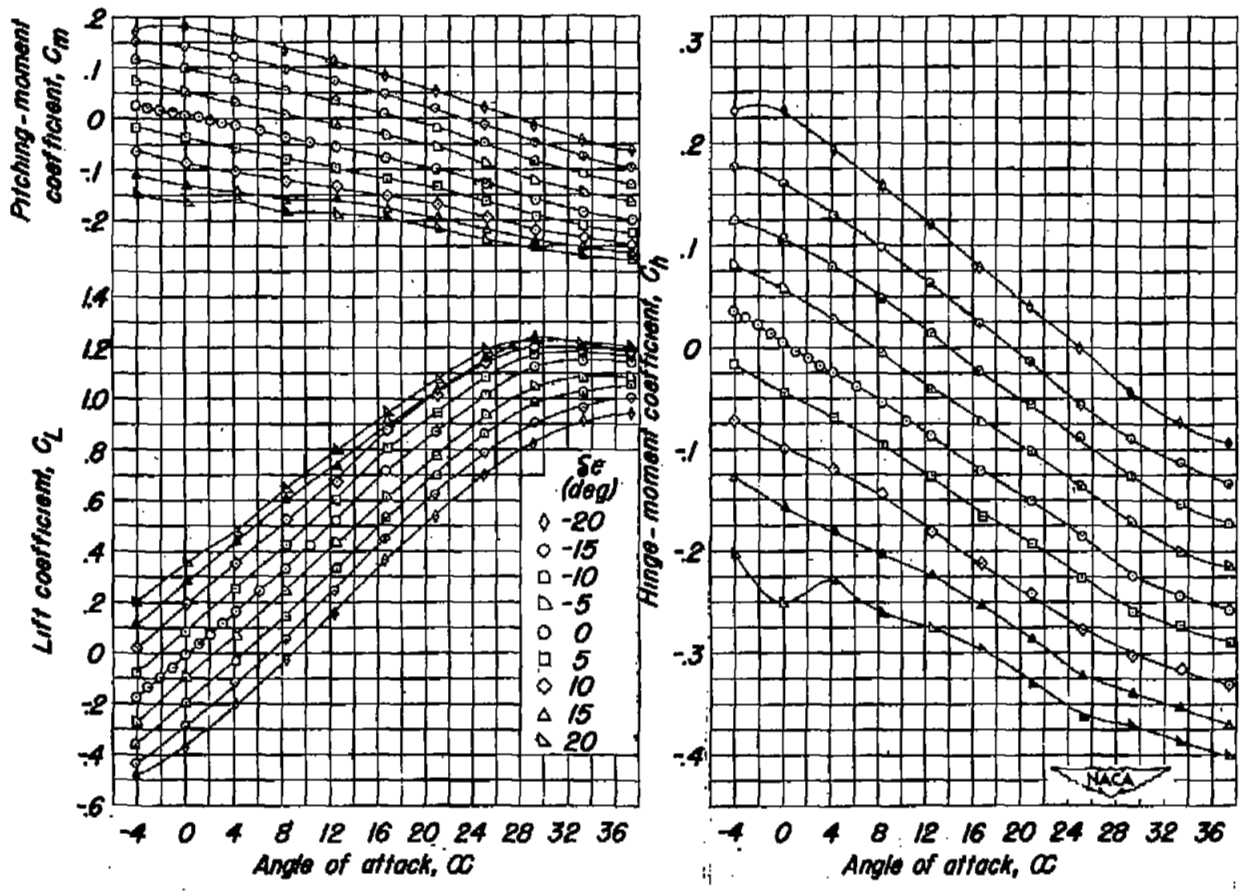


Figure 5.- Longitudinal control characteristics of complete model. Elevon with horn on; $R = 2.06 \times 10^6$; transition strips off; elevon nose gap open.

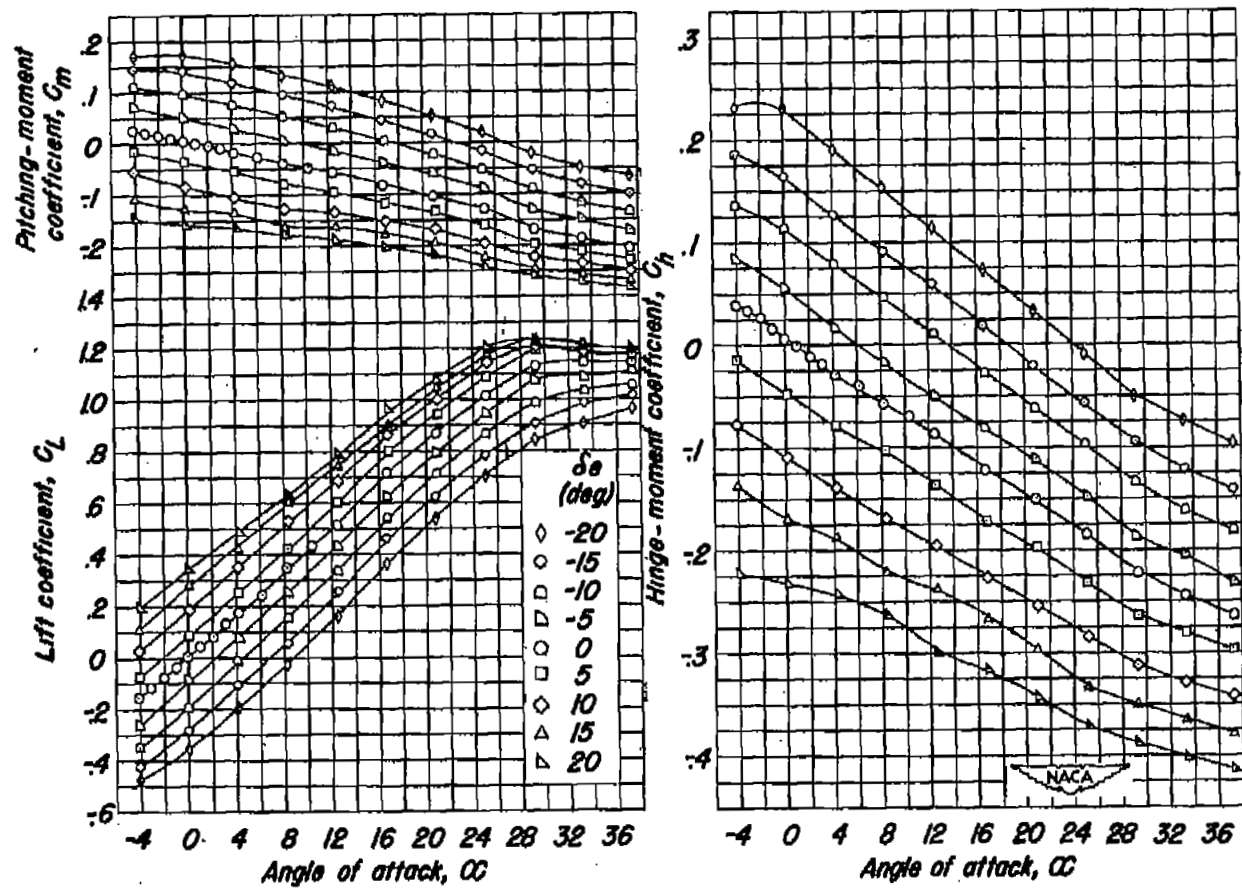


Figure 6.- Longitudinal control characteristics of complete model. Elevon with horn off; $R = 2.06 \times 10^6$; transition strips off; elevon nose gap open.

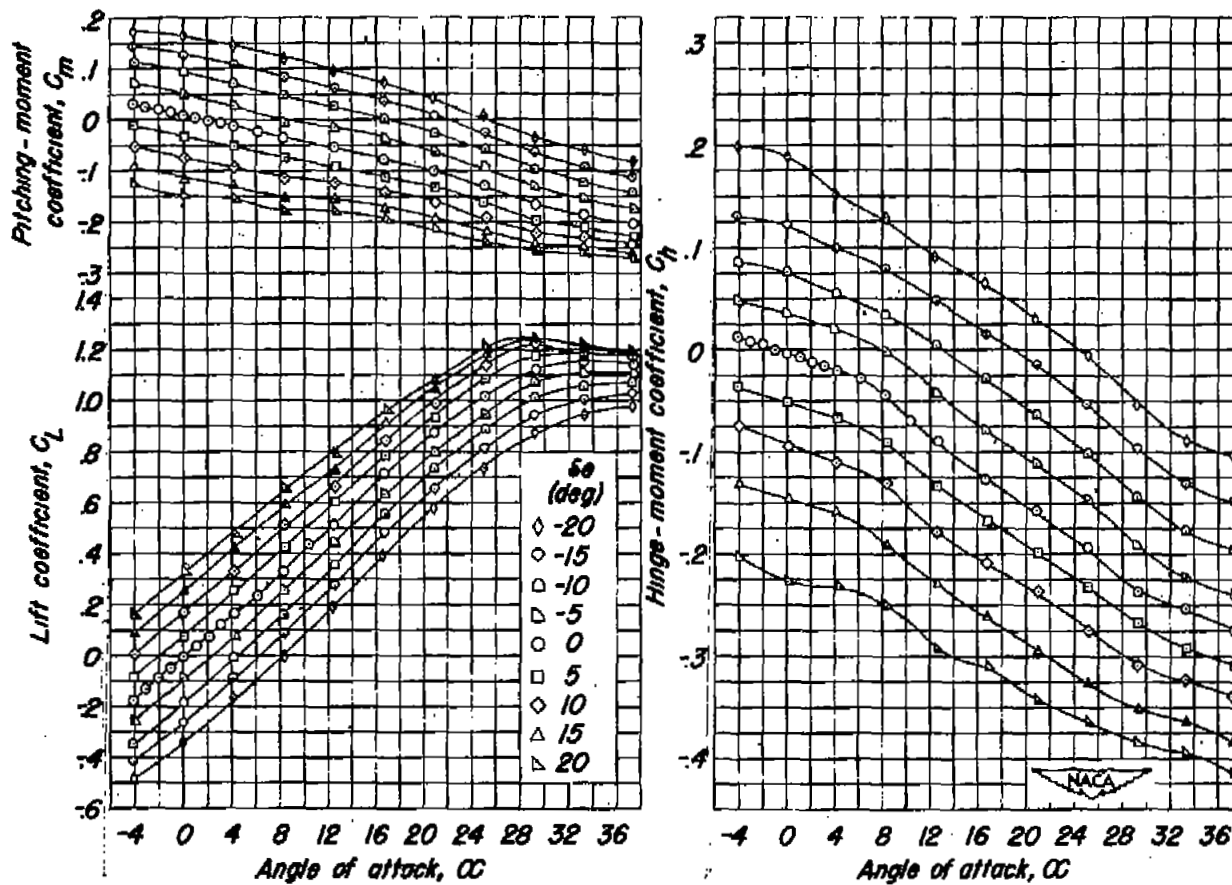


Figure 7.- Longitudinal control characteristics of complete model. Elevon with tip off; $R = 2.06 \times 10^6$; transition strips off; elevon nose gap

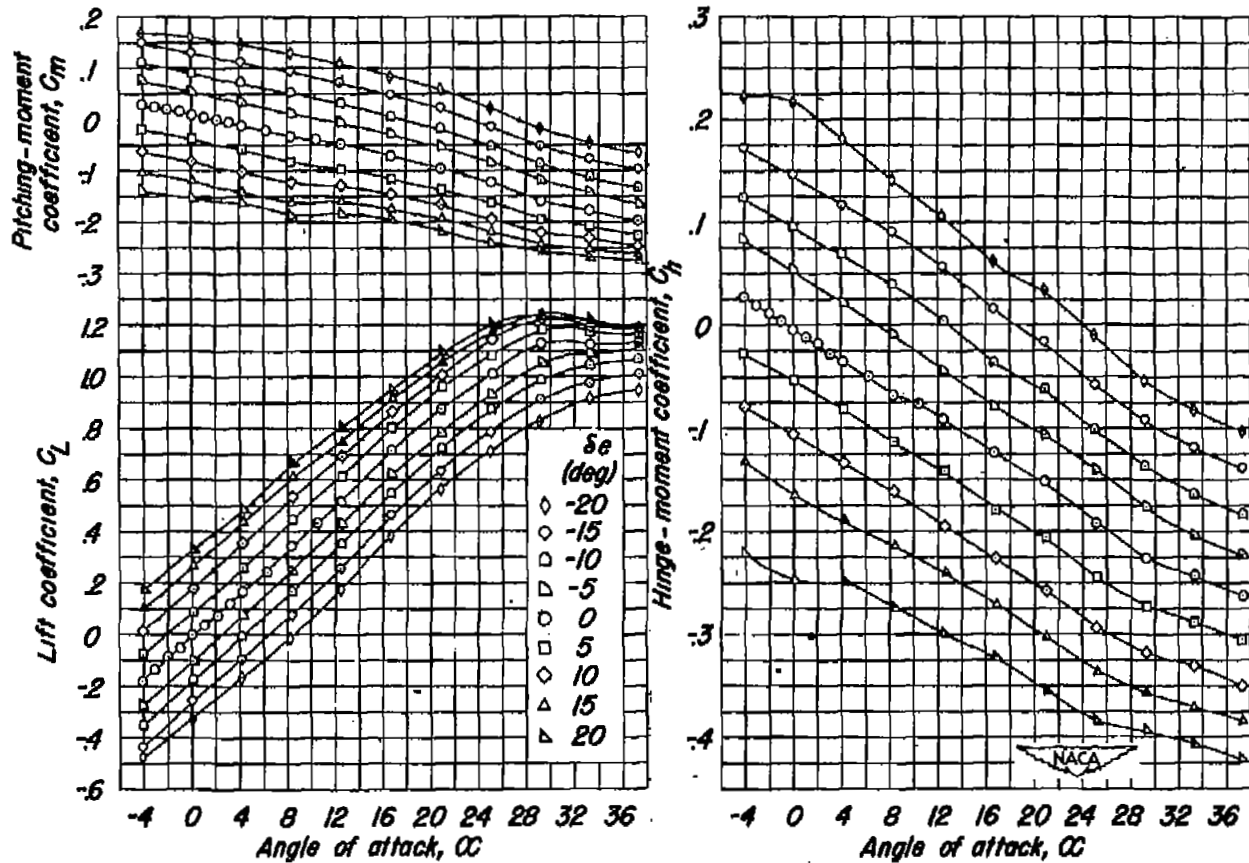


Figure 8.- Longitudinal control characteristics of complete model. Elevon with horn on; $R = 2.06 \times 10^6$; transition strips on; elevon nose gap open.

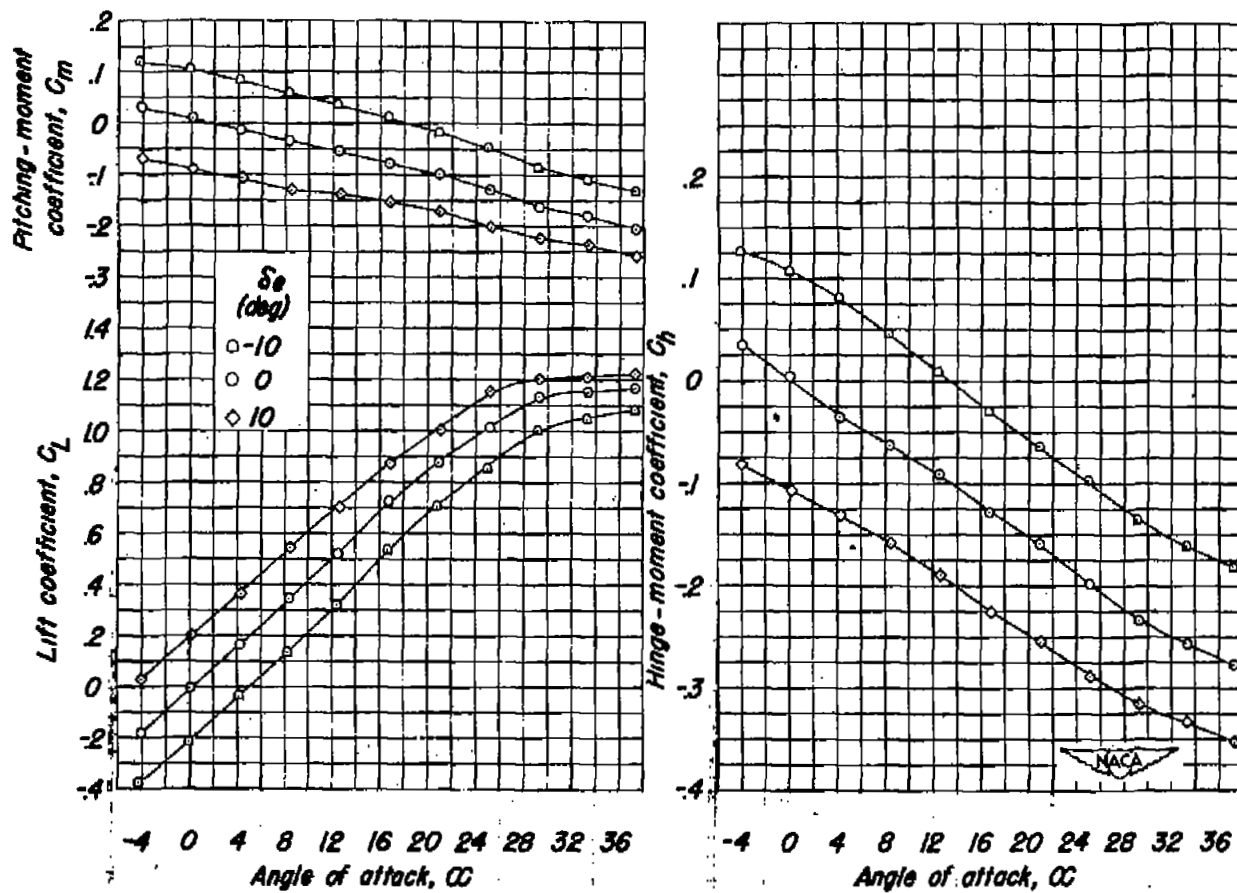


Figure 9.- Longitudinal control characteristics of complete model. Elevon with horn on; $R = 1.62 \times 10^6$; transition strips off; elevon nose gap open.

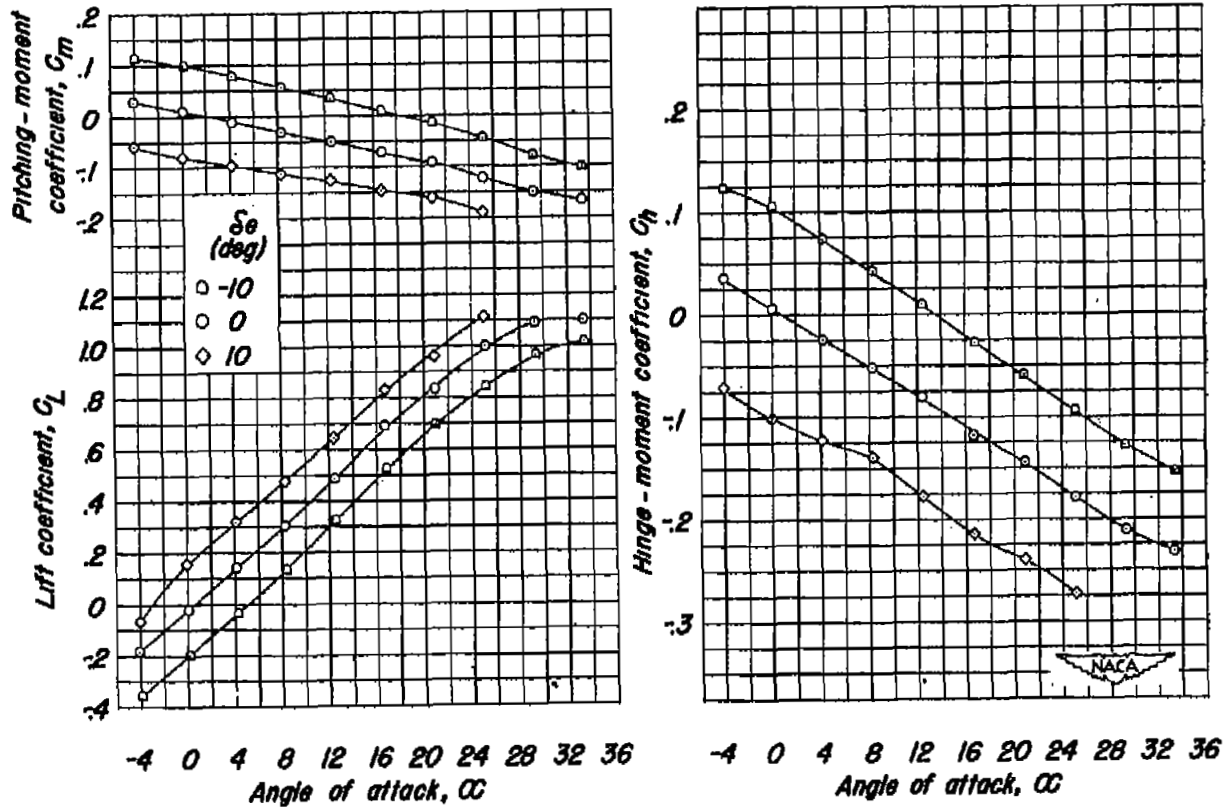


Figure 10.- Longitudinal control characteristics of complete model.
 Elevon with horn on; $R = 2.62 \times 10^6$; transition strips off; elevon nose gap open.

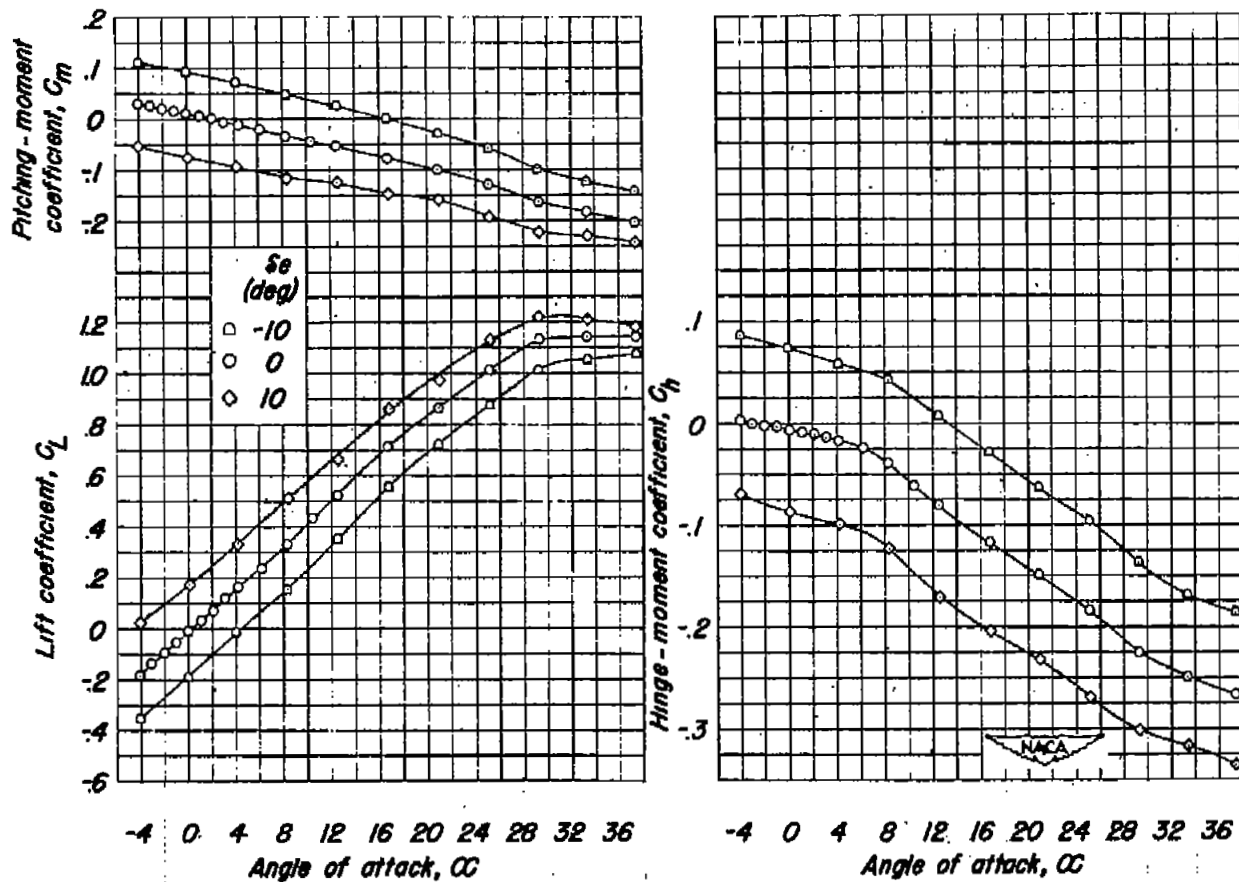
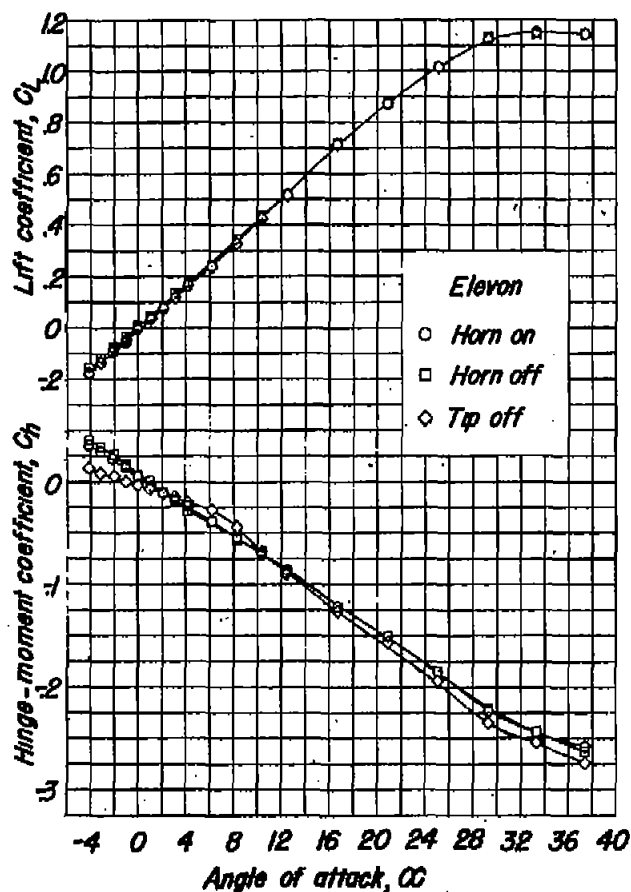
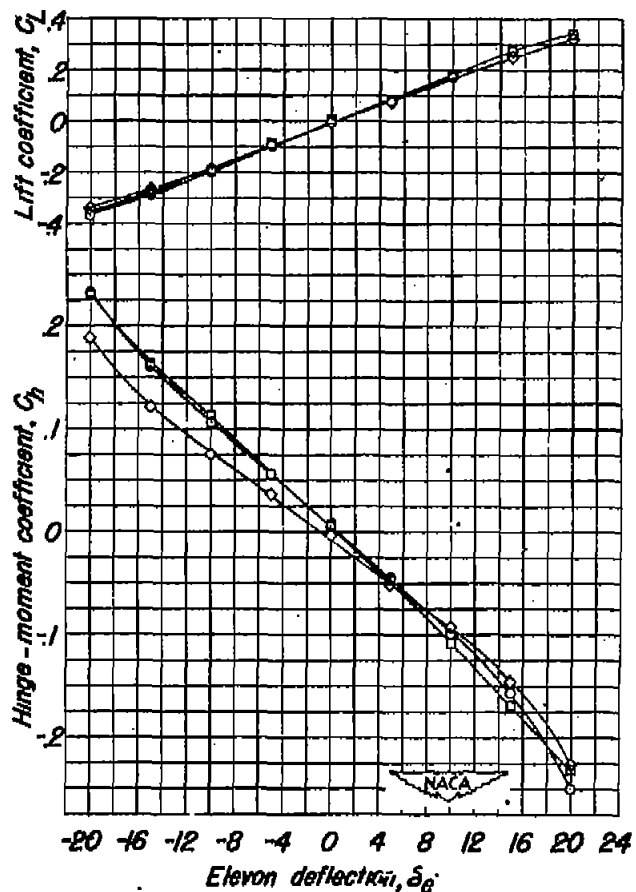


Figure 11.- Longitudinal control characteristics of complete model.
 Elevon with tip off; $R = 2.06 \times 10^6$; transition strips off; elevon nose gap sealed.

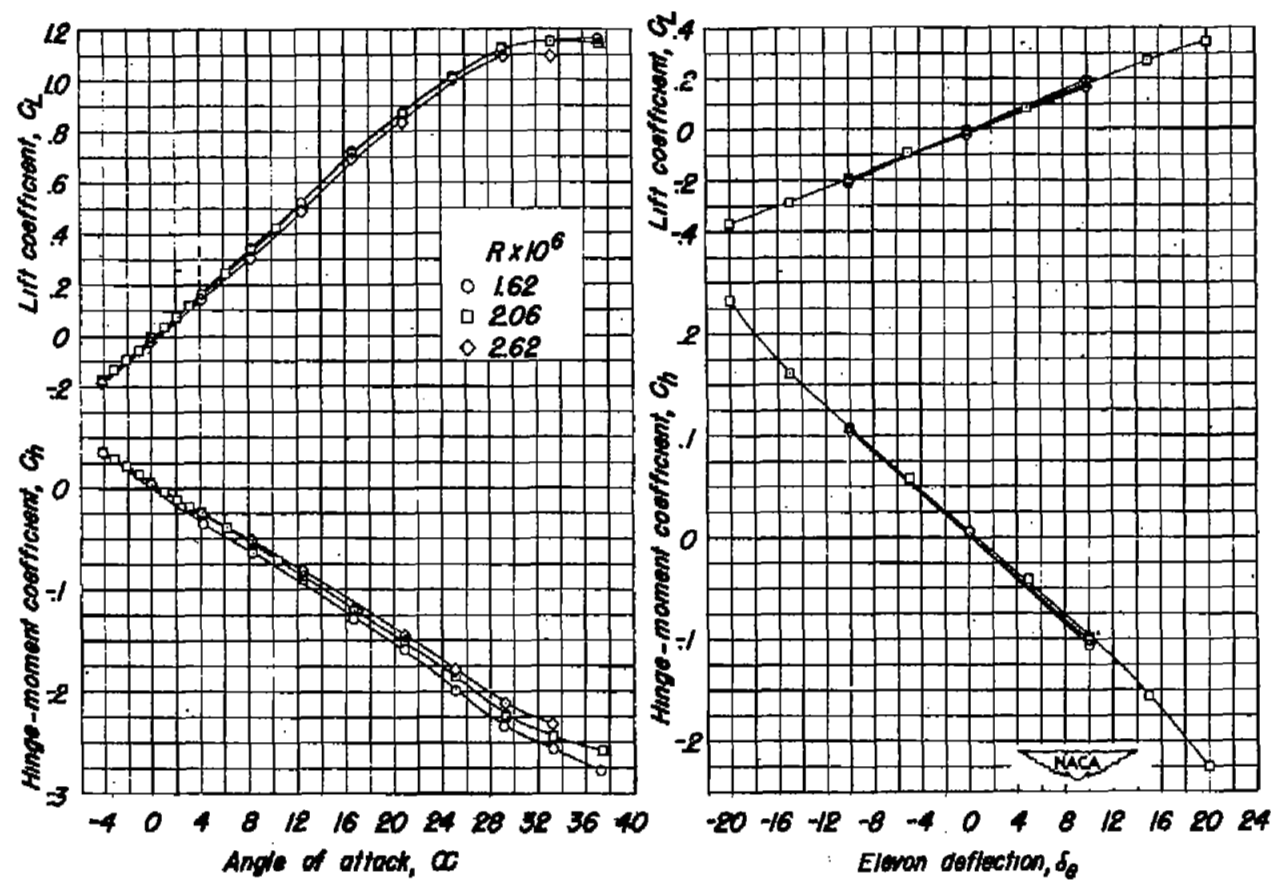


(a) C_L and C_h plotted against α , $\delta_e = 0^\circ$.



(b) C_L and C_h plotted against δ_e , $\alpha = 0^\circ$.

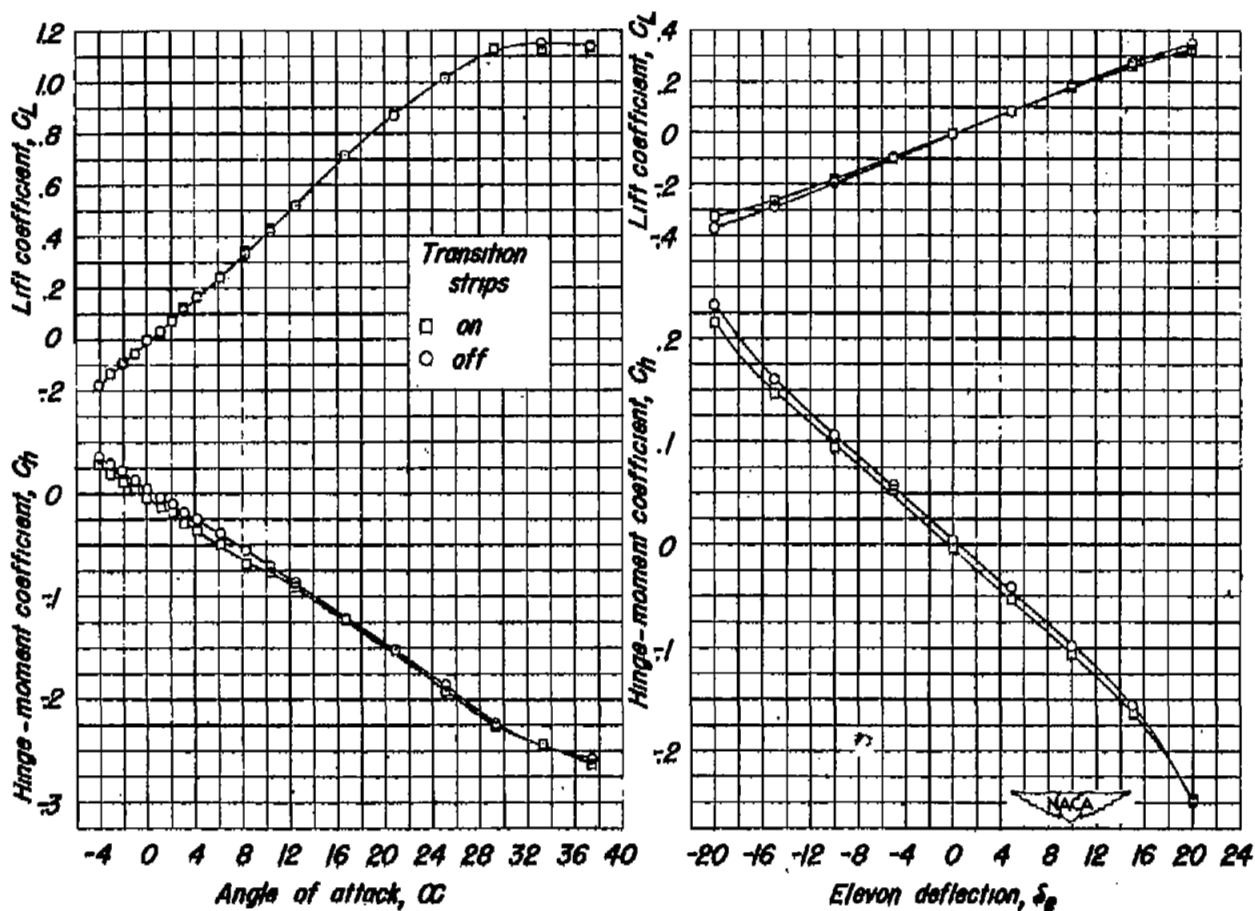
Figure 12.- Effect of elevon plan-form modifications on longitudinal control characteristics of complete model. $R = 2.06 \times 10^6$; transition strips off; elevon nose gap open.



(a) C_L and C_h plotted against α . $\delta_e = 0^\circ$.

(b) C_L and C_h plotted against δ_e . $\alpha = 0^\circ$.

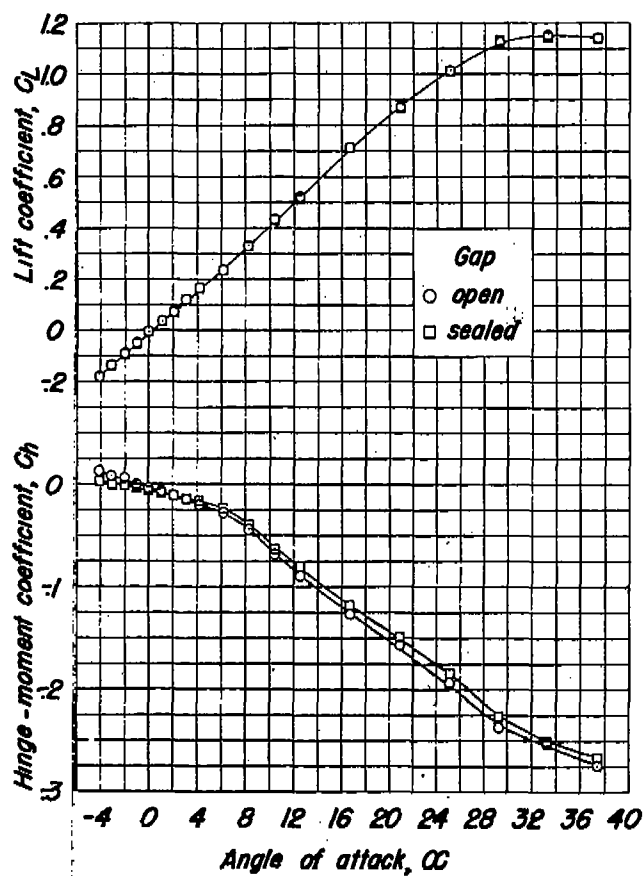
Figure 13.- Effect of Reynolds number on longitudinal control characteristics of complete model. Elevon with horn on; transition strips off; elevon nose gap open.



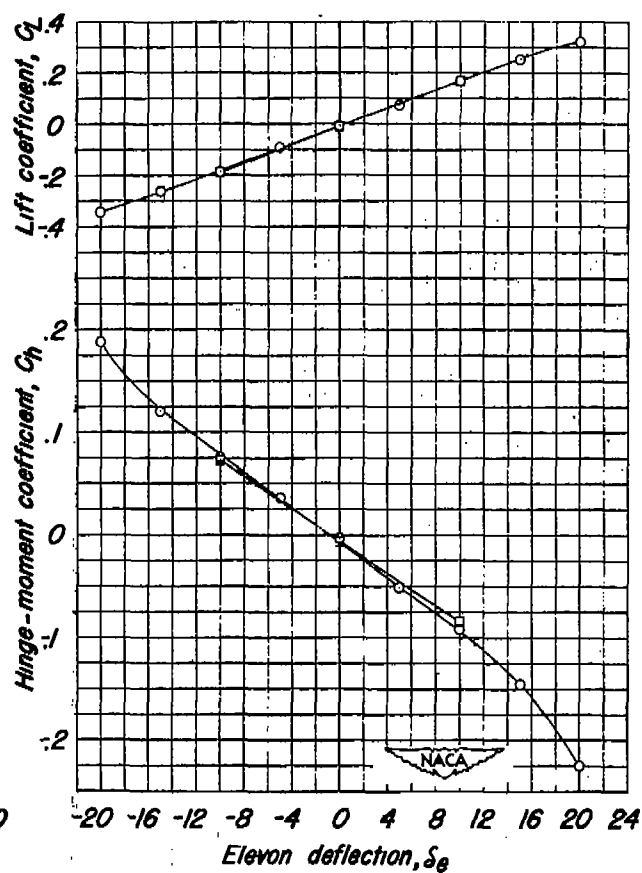
(a) C_L and C_h plotted against α . $\delta_e = 0^\circ$.

(b) C_L and C_h plotted against δ_e . $\alpha = 0^\circ$.

Figure 14.- Effect of transition strips on longitudinal control characteristics of complete model. Elevon with horn on; $R = 2.06 \times 10^6$; elevon nose gap open.



(a) C_L and C_h plotted against α . $\delta_e = 0^\circ$.



(b) C_L and C_h plotted against δ_e . $\alpha = 0^\circ$.

Figure 15.- Effect of elevon nose gap on longitudinal control characteristics of complete model. Elevon with tip off; $R = 2.06 \times 10^6$; transition strips off.

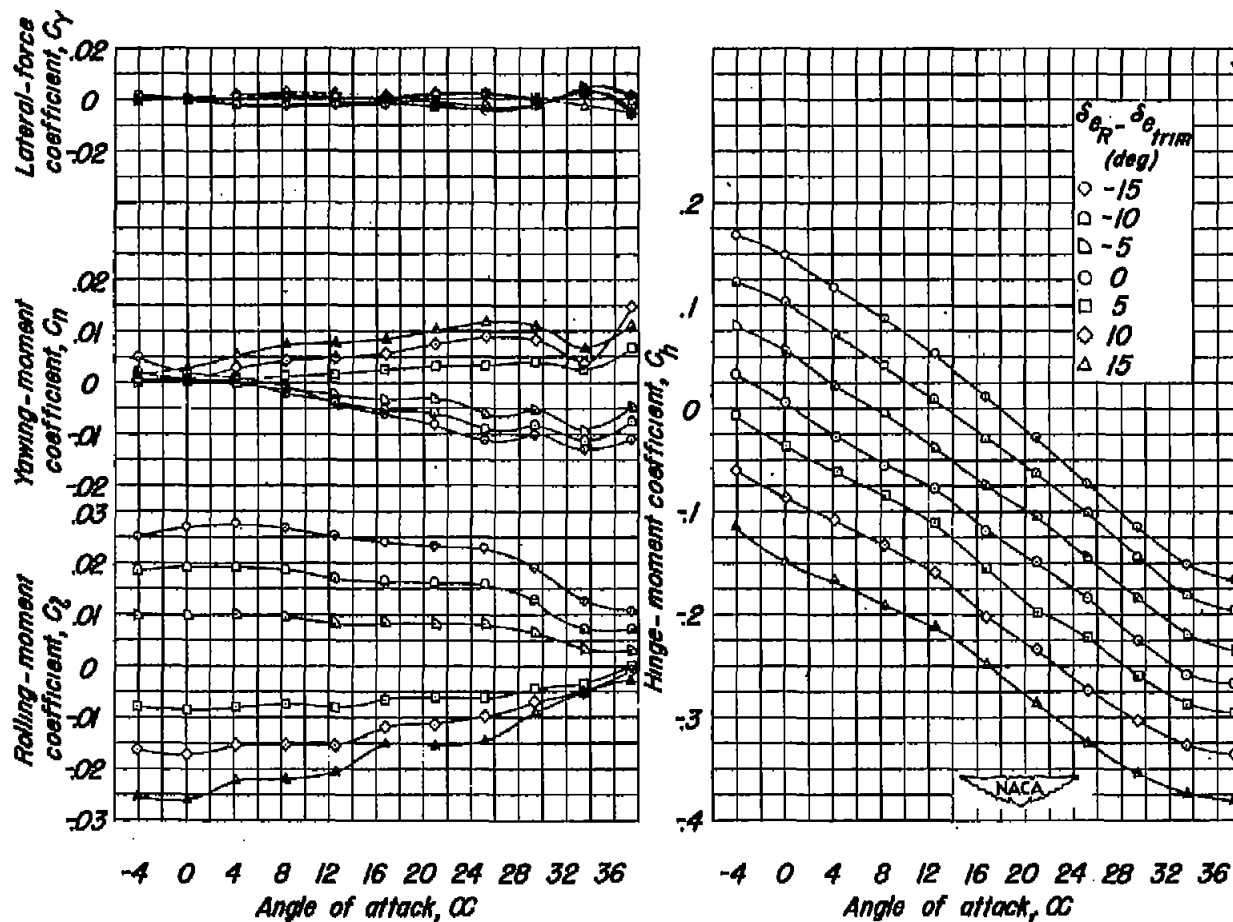


Figure 16.- Lateral control characteristics of wing alone. Elevon with horn on; $R = 2.06 \times 10^6$; transition strips off; elevon nose gap open; $\delta_{trim} = 0^\circ$.

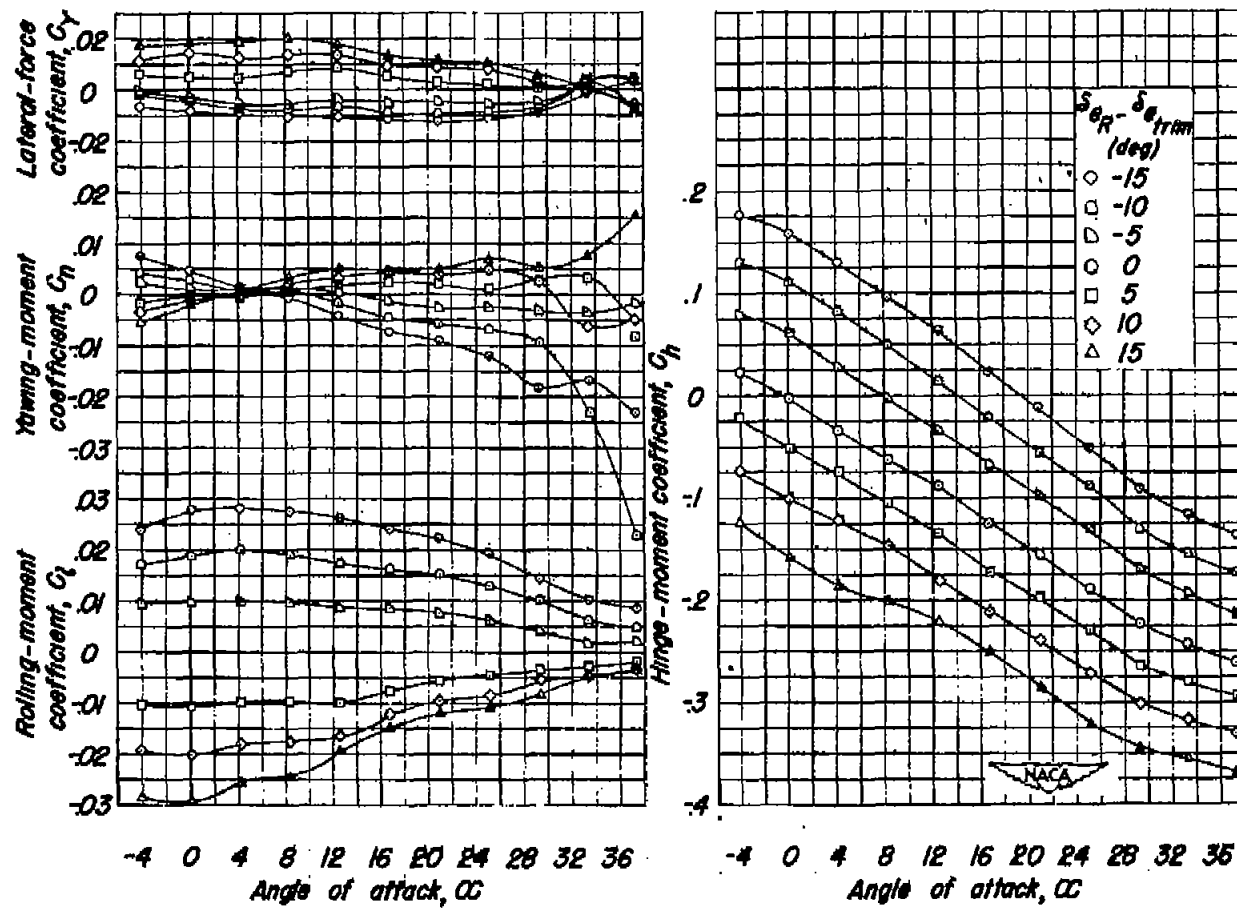


Figure 17.- Lateral control characteristics of complete model. Elevon with horn on; $R = 2.06 \times 10^6$; transition strips off; elevon nose gap open; $\delta_{trim} = 0^\circ$.

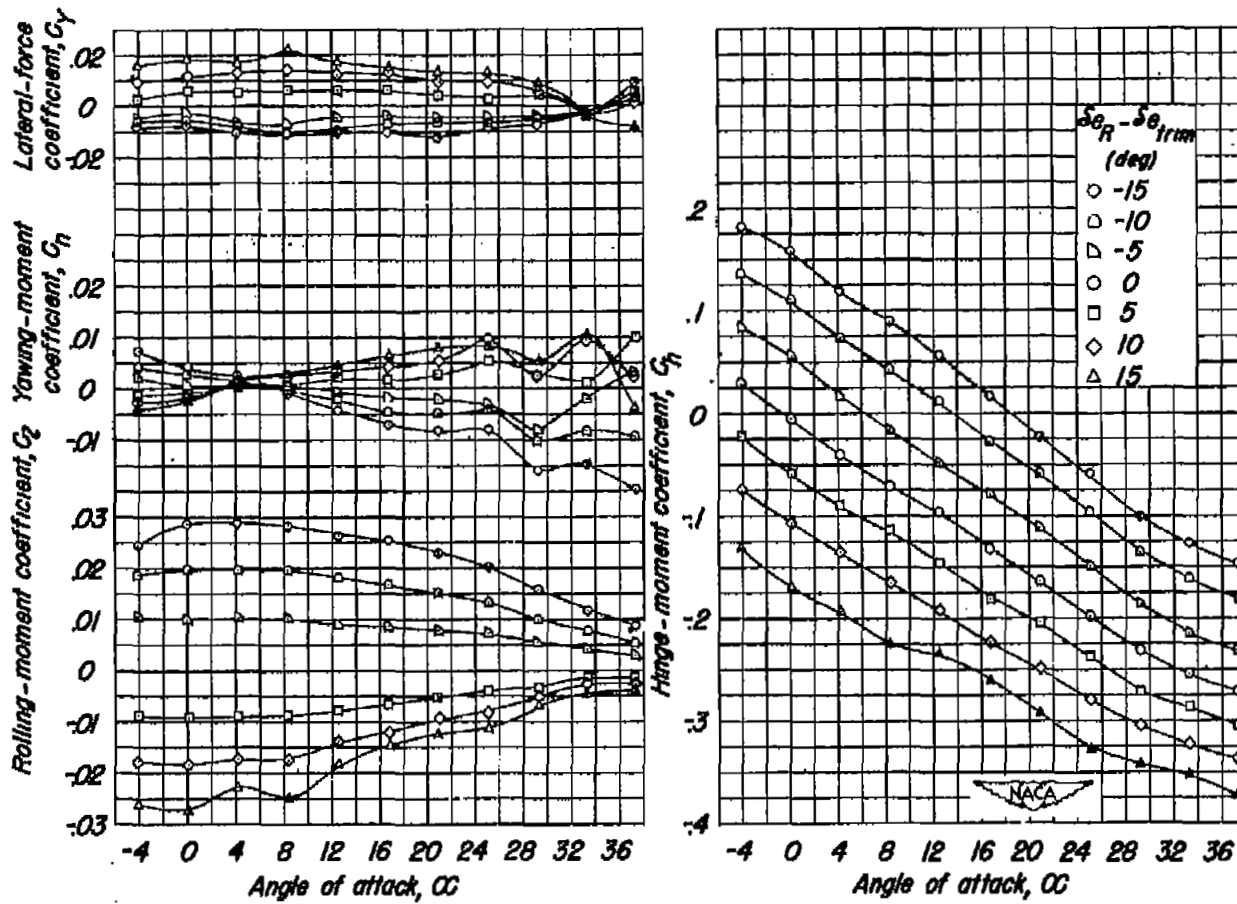


Figure 18.- Lateral control characteristics of complete model. Elevon with horn off; $R = 2.06 \times 10^6$; transition strips off; elevon nose gap open; $\delta_{eTrim} = 0^\circ$.

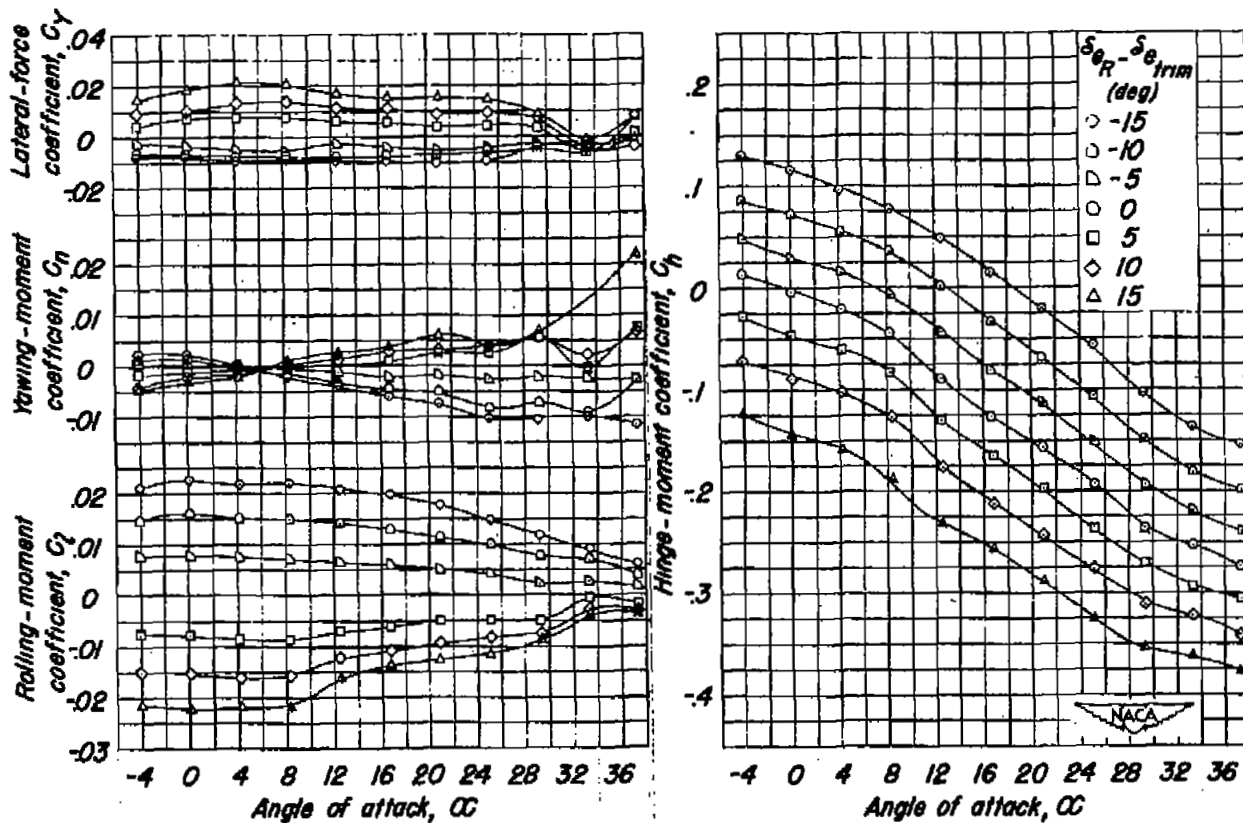


Figure 19.- Lateral control characteristics of complete model. Elevon with tip off; $R = 2.06 \times 10^6$; transition strips off; elevon nose gap open; $\delta_{e trim} = 0^\circ$.

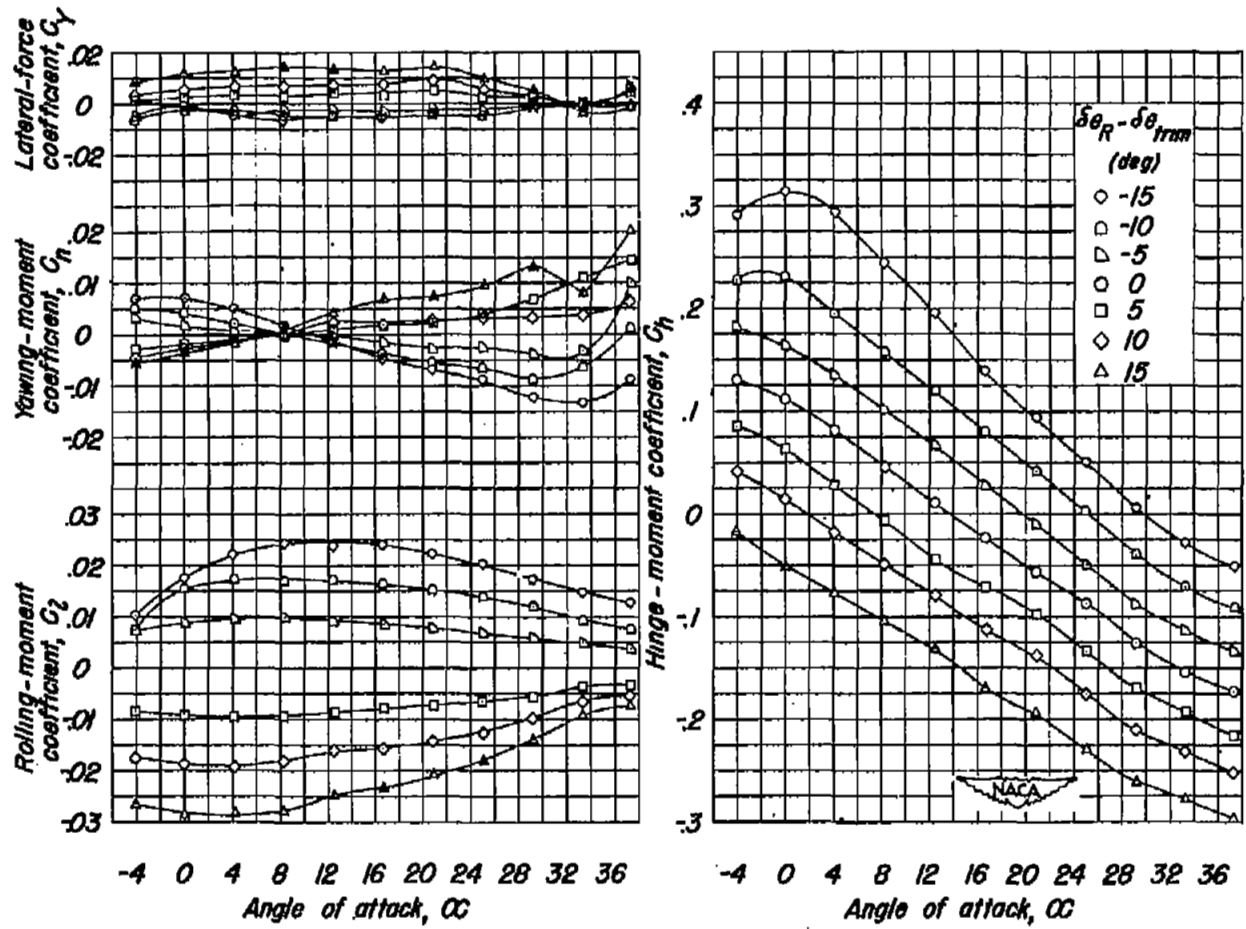
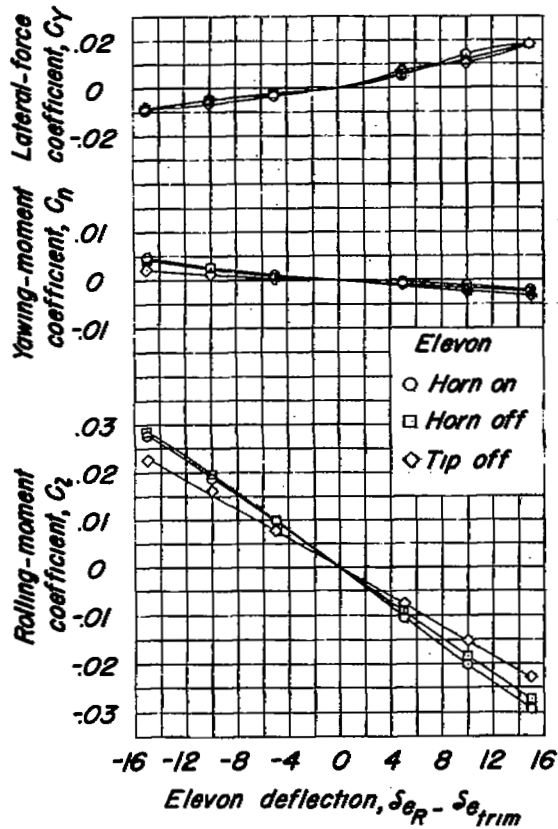
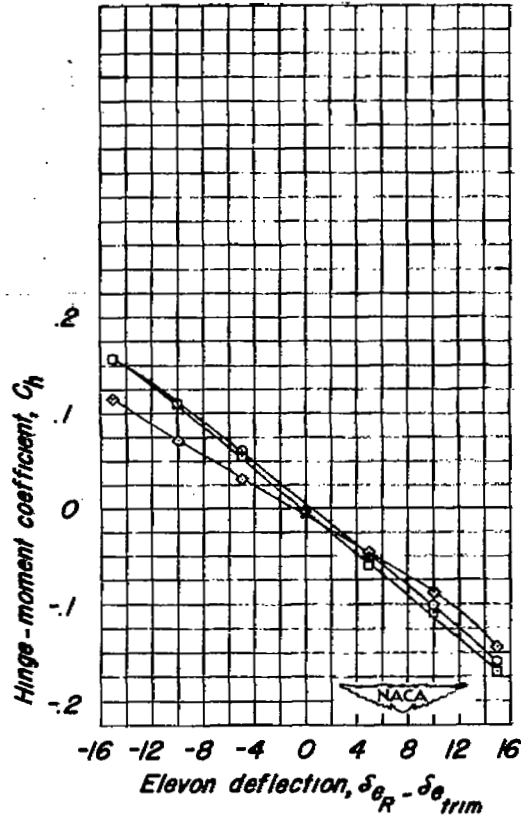


Figure 20.- Lateral control characteristics of complete model. Elevon with horn on; $R = 2.06 \times 10^6$; transition strips off; elevon nose gap open; $\delta e_{trim} = -10^\circ$.

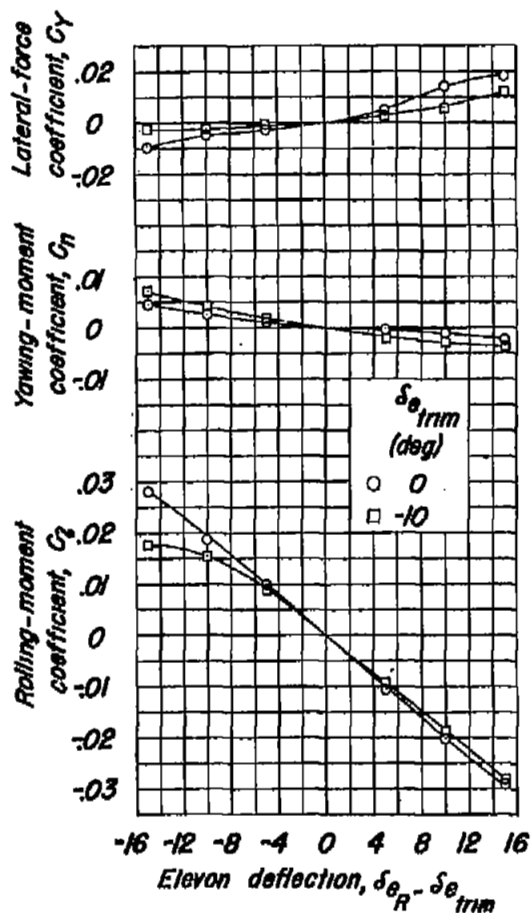


(a) C_Y , C_N , and C_L plotted against $\delta_{eR} - \delta_{eTrim}$.

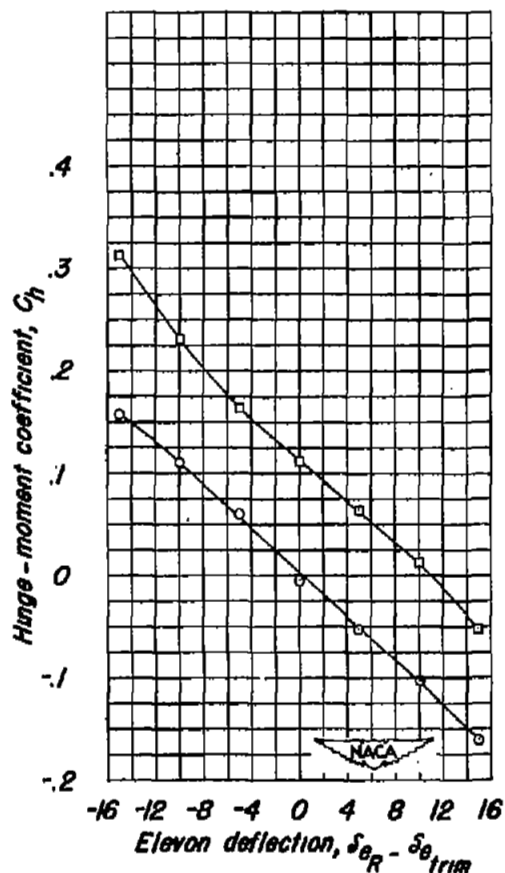


(b) C_H plotted against $\delta_{eR} - \delta_{eTrim}$.

Figure 21.- Effect of elevon plan-form modifications on lateral control characteristics of complete model. $R = 2.06 \times 10^6$; transition strips off; elevon nose gap open; $\delta_{eTrim} = 0^\circ$; $\alpha = 0^\circ$.



(a) C_Y , C_n , and C_l plotted against $\delta_{eR} - \delta_{e_{trim}}$.



(b) C_h plotted against $\delta_{eR} - \delta_{e_{trim}}$.

Figure 22.- Effect of elevon trim deflection on lateral control characteristics of complete model. Elevon with horn on; $R = 2.06 \times 10^6$; transition strips off; elevon nose gap open; $\alpha = 0^\circ$.